
Research Articles: Cellular/Molecular

Light-activated ROS production induces synaptic autophagy

Sheila Hoffmann¹, Marta Orlando^{2,3}, Ewa Andrzejak¹, Christine Bruns¹, Thorsten Trimbuch^{2,3}, Christian Rosenmund^{2,3}, Craig C. Garner^{1,2} and Frauke Ackermann¹

¹German Center for Neurodegenerative Diseases (DZNE), Charitéplatz 1, 10117 Berlin, Germany

²Charité— Universitätsmedizin Berlin, Institute of Neurobiology, Charitéplatz 1, 10117 Berlin, Germany

³NeuroCure Cluster of Excellence, Charité— Universitätsmedizin Berlin, Charitéplatz 1, 10117 Berlin, Germany

<https://doi.org/10.1523/JNEUROSCI.1317-18.2019>

Received: 24 May 2018

Revised: 10 January 2019

Accepted: 10 January 2019

Published: 17 January 2019

Author contributions: S.H., C.R., C.C.G., and F.A. designed research; S.H., M.O., E.A., C.B., and T.T. performed research; S.H., E.A., and C.B. analyzed data; S.H. wrote the first draft of the paper; S.H., M.O., C.R., C.C.G., and F.A. edited the paper; C.C.G. and F.A. wrote the paper.

Conflict of Interest: The authors declare no competing financial interests.

We would like to thank Prof. Eckart D. Gundelfinger and Noam E. Ziv for discussion and valuable comments on the manuscript, Anny Kretschmer and Katja Czielesky for technical assistance, the Virus Core Facility of the Charité- Universitätsmedizin Berlin for virus production. The work was supported by Deutsches Zentrum für Neurodegenerative Erkrankungen (DZNE), the Federal Government of Germany (DFG) SFB958 to CCG.

Correspondence should be addressed to co-corresponding authors: frauke.ackermann@dzne.de, craig-curtis.garner@dzne.de German Center for Neurodegenerative Diseases (DZNE), Charité Medical University, Charitéplatz 1, 10117 Berlin, Germany

Cite as: J. Neurosci 2019; 10.1523/JNEUROSCI.1317-18.2019

Alerts: Sign up at www.jneurosci.org/alerts to receive customized email alerts when the fully formatted version of this article is published.

Light-activated ROS production induces synaptic autophagy

Sheila Hoffmann¹, Marta Orlando^{2,3,#}, Ewa Andrzejak^{1,#}, Christine Bruns¹,
Thorsten Trimbuch^{2,3}, Christian Rosenmund^{2,3}, Craig C. Garner^{1,2,*} and Frauke
Ackermann^{1,*}

¹German Center for Neurodegenerative Diseases (DZNE), Charitéplatz 1, 10117 Berlin, Germany

²Charité – Universitätsmedizin Berlin, Institute of Neurobiology, Charitéplatz 1, 10117 Berlin, Germany

³NeuroCure Cluster of Excellence, Charité – Universitätsmedizin Berlin, Charitéplatz 1, 10117 Berlin, Germany

#authors contributed equally

*co-corresponding authors: frauke.ackermann@dzne.de, craig-curtis.garner@dzne.de

German Center for Neurodegenerative Diseases (DZNE), Charité Medical University, Charitéplatz 1, 10117 Berlin, Germany

Key Words: presynapse, autophagy, supernova, free radical, protein inactivation

Running Title: *Rapid induction of presynaptic autophagy*

Number of pages: 46

Number of figures: 11

Number of words: Abstract 214 words, Introduction 641 words, Discussion 1499 words

Author contributions: S. Hoffmann performed the majority of the experiments and analyzed data. S. Hoffmann, F. Ackermann, C. Rosenmund and C.C. Garner designed experiments. M. Orlando performed electron microscopy studies, E. Andrzejak performed electrophysiology experiments and C. Bruns performed Western Blot studies. Vectors were generated by S. Hoffmann and T. Trimbuch. S. Hoffmann, F. Ackermann and C.C. Garner wrote the manuscript.

The authors declare no competing financial interests.

Acknowledgments: We would like to thank Prof. Eckart D. Gundelfinger and Noam E. Ziv for discussion and valuable comments on the manuscript, Anny Kretschmer and Katja Czeselsky for technical assistance, the Virus Core Facility of the Charité - Universitätsmedizin Berlin for virus production. The work was supported by Deutsches Zentrum für Neurodegenerative Erkrankungen (DZNE), the Federal Government of Germany (DFG) SFB958 to CCG.

37 **Abstract**

38 The regulated turnover of synaptic vesicle (SV) proteins is thought to involve the ubiquitin-
39 dependent tagging and degradation through endo-lysosomal and autophagy pathways. Yet, it remains
40 unclear which of these pathways are used, when they become activated and whether SVs are cleared
41 en-mass together with SV proteins or whether both are degraded selectively. Equally puzzling is how
42 quickly these systems can be activated and whether they function in real-time to support synaptic
43 health. To address these questions, we have developed an imaging based system that simultaneously
44 tags presynaptic proteins while monitoring autophagy. Moreover, by tagging SV proteins with a light-
45 activated reactive oxygen species (ROS) generator, Supernova (SN), it was possible to temporally
46 control the damage to specific SV proteins and assess their consequence to autophagy mediated
47 clearance mechanisms and synaptic function. Our results show that, in mouse hippocampal neurons of
48 either sex, presynaptic autophagy can be induced in as little as 5-10 minutes and eliminates primarily
49 the damaged protein rather than the SV en-mass. Importantly, we also find that autophagy is essential
50 for synaptic function, as light-activated damage to e.g. Synaptophysin only compromises synaptic
51 function when autophagy is simultaneously blocked. These data support the concept that presynaptic
52 boutons have a robust highly regulated clearance system to maintain not only synapse integrity, but
53 also synaptic function.

54

55 **Significance Statement**

56 The real-time surveillance and clearance of synaptic proteins is thought to be vital to the health,
57 functionality and integrity of vertebrate synapses and is compromised in neurodegenerative
58 disorders, yet the fundamental mechanisms regulating these systems remain enigmatic. Our analysis
59 reveals that presynaptic autophagy is a critical part of a real-time clearance system at synapses
60 capable of responding to local damage of SV proteins within minutes and to be critical for the ongoing
61 functionality of these synapses. These data indicate that synapse autophagy is not only locally
62 regulated but also crucial for the health and functionality of vertebrate presynaptic boutons.

63

64 **Introduction**

65 The integrity of vertebrate synapses requires robust cellular programs that monitor the activity
 66 states of thousands of proteins, eliminating those that are mis-folded or damaged. Failure of these
 67 programs can lead to the accumulation of non-functional proteins that reduce the efficiency of
 68 synaptic transmission and promote neurodegeneration (Liang and Sigrist, 2018; Vijayan and
 69 Verstreken, 2017; Waites et al., 2013). Neurons are endowed with several surveillance and clearance
 70 systems. These include an ubiquitin based tagging system that conjugates ubiquitin chains to damaged
 71 proteins, as well as several degradative systems that, for example, eliminate soluble proteins via the
 72 proteasome or integral membrane proteins and protein aggregates via the endo-lysosomal and/or
 73 autophagy systems (Wang et al., 2017).

74 Given their distance from the cell soma and high metabolic demand, synapses pose a significant
 75 challenge to neurons, as they have to maintain and ensure a stable functional pool of proteins
 76 (Tammineni et al., 2017). How might this be achieved? Emerging data indicate that synapses utilize
 77 their own local machinery to eliminate proteins e.g. in response to changes in synaptic activity or
 78 homeostatic plasticity (Vijayan and Verstreken, 2017). For example, the ESCRT machinery facilitates
 79 via Rab35 the elimination of subsets of SV proteins in response to changes in synaptic activity
 80 (Sheehan et al., 2016). Moreover, specific E3 ubiquitin ligases have been associated with the selective
 81 removal of key regulators of synaptic transmission such as RIM1 (Yao et al., 2007) and Munc13 by the
 82 proteasome (Jiang et al., 2010; Yi and Ehlers, 2005). Intriguingly, two active zone proteins, Piccolo and
 83 Bassoon, have also been identified as regulators of presynaptic proteostasis, as their inactivation leads
 84 to the loss of SVs and disintegration of synaptic junctions through the activation of E3 ligases (Waites
 85 et al., 2013) and autophagy (Okerlund et al., 2017).

86 Although these clearance systems are anticipated to ensure functionality of synaptic proteins, it
 87 remains unclear whether some are specialized in the removal of only subsets of synaptic proteins. A
 88 growing number of studies point to the importance of autophagy not only in maintaining
 89 mitochondrial health, but also the clearance of aggregated proteins (Vijayan and Verstreken, 2017).
 90 Interestingly, in Alzheimer's disease brains, an up-regulation of autophagy has been observed (Boland
 91 et al., 2008; Lee et al., 2010; Nixon et al., 2005), however, in other diseases characterized by aggregate-

prone proteins such as Parkinson's and Huntington's disease, autophagy is not engaged (Martinez-Vicente et al., 2010; Nixon, 2013; Rubinsztein et al., 2012; Spencer et al., 2009), which might contribute to the accumulation of protein aggregates and subsequent reduced neuronal survival (Ebrahimi-Fakhari et al., 2011; Nixon, 2013; Yue et al., 2009). This latter concept is supported by the analysis of Atg5 or Atg7 knockout mice, two essential autophagy-related proteins, which exhibit hallmarks of neurodegeneration (Hara et al., 2006; Komatsu et al., 2006). Defining the role of degradative systems during health and disease requires a better understanding of when and where each is turned on and which subsets of proteins they eliminate. For example, those critical for the real-time maintenance of synaptic function should be locally regulated and operating on a second to minute time scale, while those responding to chronic damage may act on longer time scales like hours. To address these fundamental questions, we have developed a strategy to selectively damage SV proteins within presynaptic boutons. This was accomplished by tethering the light-activated free radical oxygen species (ROS) generator Supernova (Takemoto et al., 2013) to different SV proteins, allowing the local light-activated ROS-mediated damage of SV proteins with a half-radius of photo-damage as small as 3-4nm (Takemoto et al., 2013).

This manipulation was found to rapidly and selectively induce presynaptic autophagy within 5 minutes and lead primarily to the elimination of damaged proteins and not SV proteins en-mass. Moreover, the selective damage of SV proteins allowed us to show that presynaptic autophagy is critical for the real-time maintenance of synaptic transmission.

112 **Material and Methods**

113 *Construction of vectors:* Monitoring of autophagy within presynaptic boutons was achieved by creating
 114 a set of lentiviral expression vectors. All vectors are based on the commercially available vector FUGW
 115 (plasmid #14883, Addgene). In order to co-express mCherry-tagged Synaptophysin (Syp) and eGFP-
 116 LC3, Synaptophysin-mCherry (Synaptophysin, NM_012664.3) was synthesized by Eurofins Genomics
 117 with a downstream glycine linker that was fused to a self-cleaving 2A peptide (Kim et al., 2011). This
 118 element was then exchanged with GFP in the FUGW vector by ligation. Subsequently, the eGFP-LC3
 119 (LC3, U05784.1) segment from FU-ptf-LC3 (Okerlund et al., 2017) was subcloned in frame after the
 120 P2A sequence, which resulted in the vector FU-Syp-mCherry-P2A-eGFP-LC3. This vector also served as
 121 a template for tagging Synaptophysin with Supernova. Here, Supernova was synthesized by Eurofins
 122 Genomics (Supernova, AB522905) (Takemoto et al., 2013) and exchanged for mCherry forming FU-
 123 Syp-Supernova-P2A-eGFP-LC3. For the simultaneous expression of a short hairpin RNA to knock down
 124 Atg5 transcripts, a U6 promoter driven shRNA cassette was cloned upstream of the ubiquitin
 125 promoter. The shRNA (5'-CCA TCT GAG CTA CCC AGA TAA TTC AAG AGA TTA TCT GGG TAG CTC AGA
 126 TTT TTT TGG AA-3') was cloned into the vector to form F-U6-shAtg5-U-Syp-Supernova-P2A-eGFP-
 127 LC3. A scrambled shRNA against rat Clathrin served as negative control (F-U6-scRNA(SC)-U-Syp-
 128 Supernova-P2A-eGFP-LC3). In order to express Supernova within the lumen of SVs, we inserted
 129 Supernova cDNA sequences at residue 184 in Synaptophysin (Syp-lumSN) together with a GSG linker,
 130 by Gibson assembly (Gibson et al., 2009) followed by subcloning to create FU-Syp-lumSN-P2A-eGFP-
 131 LC3). Ligation of a PCR amplified Supernova transcript at the C-terminus of Synaptophysin and after
 132 the downstream sequence of eGFP-LC3 generated the eGFP-LC3 empty vector FU-Syp-Supernova. To
 133 monitor endo-lysosomal systems PCR amplified Rab7 (XM_005632015.2) was exchanged with LC3 in
 134 FU-Syp-Supernova-P2A-eGFP-LC3 by Gibson assembly creating FU-Syp-Supernova-P2A-eGFP-Rab7.
 135 Lentiviral vectors expressing eGFP-LC3 and either Supernova tagged Synapsin (Syn) (NM_019133) or
 136 Synaptotagmin (Syt) (NM_001252341) (FU-Syn-Supernova-P2A-eGFP-LC3 and FU-Syt-Supernova-
 137 P2A-eGFP-LC3) were created by PCR amplification of Synapsin or Synaptotagmin from plasmid DNA
 138 (Chang et al., 2018; Waites et al., 2013) before being subjected to a Gibson assembly reaction with the
 139 purified Syp-deleted FU-Syp-Supernova-P2A-eGFP-LC3 vector. The vector FU-eGFP-LC3 was created

140 by exchanging GFP in the FUGW vector with the eGFP-LC3 (LC3, U05784.1) segment from FU-ptf-LC3
 141 (Okerlund et al., 2017). All final constructs were verified by both restriction digest and sequencing.

142

143 *HeLa/HEK293 cell culture and infection:* HeLa (RRID:CVCL_0030)/HEK293 (RRID:CVCL_0045) cells
 144 were maintained in DMEM complete medium (DMEM, 10% FCS, 1% P/S) (Thermo Fisher Scientific,
 145 Waltham, USA). Medium was exchanged every 2 to 4 days. HeLa/HEK293 cells were routinely
 146 passaged at 80% confluence. Cells were washed with PBS and subsequently treated with 0.05%
 147 Trypsin-EDTA (Thermo Fisher Scientific, Waltham, USA) for 1 min at 37°C. Trypsin was inhibited
 148 using DMEM complete medium, afterwards cells were detached from the flask, counted and re-plated
 149 at a density of 30k per 1cm² onto glass coverslips. For the autophagy induction assays, HeLa cells were
 150 infected with lentivirus (FU-Syp-mCherry-P2A-eGFP-LC3) 24 hours after plating by adding 100µl per
 151 6-well. 3 days after infection, DMEM was exchanged to EBSS medium (Thermo Fisher Scientific,
 152 Waltham, USA) containing 100µM chloroquine (in H₂O, Sigma-Aldrich, St. Louis, USA) for 2 hours at
 153 37°C, in order to enhance the visualization of autophagy by blocking lysosomal degradation. Control
 154 cells were left untreated.

155

156 *Immunocytochemistry of HeLa cells:* Cells were fixed with 4% PFA in PBS for 4 min at RT and washed
 157 with PBS twice. All following steps were performed at RT. Cells were permeabilized by three washing
 158 steps with PBS + 0.2% Tween-20 (PBS-T) for a total of 30 min followed by incubation with PBS-T with
 159 5% normal goat serum (NGS) (=blocking solution) for another 30 min. The primary antibody was
 160 diluted in blocking solution and cells were incubated in this solution for 45 min. The following
 161 antibodies were used: primary antibodies against LC3 (RRID: AB_2274121) (1:500; rabbit; MBL
 162 International, Woburn, USA; Cat# PM036), p62 (RRID: AB_398152) (1:200; mouse; BD, Heidelberg,
 163 Germany; Cat# 610833). Afterwards cells were washed three times in PBS-T for 10 min each. The
 164 secondary antibody, diluted in PBS-T 1:1000 (RRID: AB_141725, RRID: AB_2535813) (Thermo Fisher
 165 Scientific, Waltham, USA), was put onto the cells for 60 min and washed away twice with PBS-T and
 166 once with PBS for 10 min each. Finally, coverslips were mounted using ProLong Diamond Antifade
 167 Mountant (Thermo Fisher Scientific, Waltham, USA).

168

169 *Dihydroethidium assay:* HEK293 cells were seeded on a μ -Slide 8 Well (ibidi GmbH, Martinsried,
 170 Germany) culture dish with a density of 30k per 1cm^2 and transfected one day later using X-
 171 tremeGENE 9 DNA Transfection Reagent (Roche Diagnostics, Mannheim, Germany) according to the
 172 manufacturers instructions. 24-48 hours after transfection, DMEM complete medium was changed and
 173 dihydroethidium (DHE) was added to a final concentration of $10\mu\text{M}$ (in DMSO, Thermo Fisher
 174 Scientific, Waltham, USA) in DMEM complete medium. Cells were incubated with DHE for 20 min at
 175 37°C followed by two washing steps with 37°C warm PBS. Afterwards, PBS was exchanged with warm
 176 tyrodes buffer pH 7.4 (119mM NaCl, 2.5mM KCl, 25mM HEPES, 2mM CaCl_2 , 2mM MgCl_2 , 30mM
 177 glucose) and live cells were imaged in a custom-built chamber before bleaching SN, immediately after
 178 bleaching SN and 15 minutes after bleaching SN.

179

180 *Preparation of cultured hippocampal neurons:* All procedures for experiments involving animals were
 181 approved by the animal welfare committee of Charité Medical University and the Berlin state
 182 government. For live cell imaging and immunocytochemistry, hippocampal neuron cultures from
 183 mouse WT animals (C57BL/6J) (RRID: IMSR_JAX:000664) of either sex were prepared on glass
 184 coverslips using the Banker protocol (Banker, 1988; Meberg and Miller, 2003) or on μ -Slide 8 Well
 185 culture dishes (ibidi GmbH, Martinsried, Germany). For Banker cultures, astrocytes were prepared
 186 from mouse WT cortices P 0-2 and seeded on 6-well or 12-well plates at a density of 10k per 1cm^2 5-7
 187 d before the addition of neurons (see below). Neuronal cultures were prepared from hippocampi
 188 dissected from WT mice P 0-2 brains in cold Hanks' Salt Solution (Millipore, Darmstadt, Germany),
 189 followed by a 30 min incubation in enzyme solution (DMEM (Gibco, Thermo Fisher Scientific,
 190 Waltham, USA), 3.3mM Cystein, 2mM CaCl_2 , 1mM EDTA, 20U/ml Papain (Worthington, Lakewood,
 191 USA)) at 37°C . Papain reaction was inhibited by the incubation of hippocampi in inhibitor solution
 192 (DMEM, 10% fetal calf serum (FCS) (Thermo Fisher Scientific, Waltham, USA), 38mM BSA (Sigma-
 193 Aldrich, St. Louis, USA) and 95mM Trypsin Inhibitor (Sigma-Aldrich, St. Louis, USA)) for 5 min.
 194 Afterwards, cells were triturated in NBA (Neurobasal-A Medium, 2% B27, 1% Glutamax, 0.2%P/S)
 195 (Thermo Fisher Scientific, Waltham, USA) by gentle pipetting up and down. Isolated neuronal cells

196 were plated onto nitric acid washed and poly-l-lysine coated glass coverslips with paraffin dots at a
 197 density of 10k per 1cm². After 1.5 hours the coverslips were put upside down onto the prepared
 198 astrocytes and co-cultured in NBA at 37°C, 5% CO₂, for 13-15 days *in vitro* (DIV) before starting
 199 experiments. For cultures on multi-well culture dishes, dissociated hippocampal neurons were plated
 200 directly onto μ -Slide 8 Well Grid-500 ibiTreat culture dishes (ibidi GmbH, Martinsried, Germany) at a
 201 density of 25k per 1cm² and maintained in NBA at 37°C, 5% CO₂, for 13-15 DIV before starting
 202 experiments.

203
 204 *Lentivirus production:* All lentiviral particles were provided by the Viral Core Facility of the Charité -
 205 Universitätsmedizin Berlin (vcf.charite.de) and were prepared as described previously (Lois et al.,
 206 2002). Briefly, HEK293T (RRID: CVCL_0063) cells were co-transfected with 10 μ g of shuttle vector, 5 μ g
 207 of helper plasmid pCMVdR8.9, and 5 μ g of pVSV.G with X-tremeGENE 9 DNA transfection reagent
 208 (Roche Diagnostics, Mannheim, Germany). Virus containing cell culture supernatant was collected
 209 after 72 hours and filtered for purification. Aliquots were flash-frozen in liquid nitrogen and stored at
 210 -80°C. Neurons were infected with lentivirus at 2-3 DIV.

211
 212 *Immunocytochemistry of hippocampal neurons:* To chemically induce or inhibit autophagy, primary
 213 hippocampal neurons 13-15 DIV (that were infected with lentivirus at 2-3 DIV) were treated with 2 μ M
 214 rapamycin (in DMSO, Sigma-Aldrich, St. Louis, USA) and/or 1 μ M wortmannin (in DMSO, InvivoGen,
 215 San Diego, USA), respectively. Untreated cells were used as a control. After treatment, cells were fixed
 216 with 4% PFA in PBS for 4 min and washed twice with PBS (10 min each). Afterwards, cells were
 217 permeabilized with PBS + 0.2% Tween-20 (PBS-T) three times for 10 min each. Following a 30 min
 218 incubation with 5% normal goat serum (NGS) in PBS-T (=blocking solution), neurons were incubated
 219 with primary antibodies, diluted in blocking solution, for 45 min at RT. The following antibodies were
 220 used: primary antibody against p62 (RRID: AB_1279301) (1:500; rabbit; MBL International, Woburn,
 221 USA; Cat# PM045), Homer1 (RRID: AB_10549720) (1:1000; guinea pig; Synaptic Systems; Göttingen,
 222 Germany; Cat# 160004), Killerred (recognizes Supernova) (1:1000; rabbit; Evrogen, Moscow, Russia;
 223 Cat# AB961), GFP (RRID: AB_2534023) (1:1000; chicken; Thermo Fisher Scientific, Waltham, USA;

224 Cat# A10262), mCherry (RRID: AB_2571870) (1:1000; rabbit; Abcam, Cambridge, UK; Cat#
 225 ab167453), LC3 (RRID: AB_796155) (1:500; rabbit; Sigma-Aldrich, St. Louis, USA; Cat# L7543),
 226 Bassoon (RRID: AB_2290619) (1:500; guinea pig; Synaptic Systems, Göttingen, Germany; Cat#
 227 141004), Synaptotagmin1 (RRID: AB_887832) (1:1000; mouse; Synaptic Systems, Göttingen,
 228 Germany; Cat# 105011), Synaptophysin1 (RRID: AB_887824) (1:1000; mouse; Synaptic Systems,
 229 Göttingen, Germany; Cat# 101011), Synapsin1 (RRID: AB_1281135) (1:1000; rabbit; Abcam,
 230 Cambridge, UK; Cat# ab64581), Chmp2b (RRID: AB_2079471) (1:200; rabbit; Abcam, Cambridge, UK;
 231 Cat# ab33174). Afterwards cells were washed three times in PBS-T for 10 min each, incubated with
 232 the secondary antibody, diluted in PBS-T 1:1000 (RRID: AB_142924, RRID: AB_25762179, RRID:
 233 AB_141725, RRID: AB_141882, RRID: AB_10563566, RRID: AB_2535813, RRID: AB_1500630, RRID:
 234 AB_144696) (Thermo Fisher Scientific, Waltham, USA), for 60 min and washed twice with PBS-T and
 235 once with PBS for 10 min each. Finally, coverslips were dipped in H₂O and mounted in ProLong
 236 Diamond Antifade Mountant (Thermo Fisher Scientific, Waltham, USA).

237

238 *Western Blot analyses:* Cultured hippocampal neurons, either infected with lentivirus at 2-3 DIV (TD)
 239 or uninfected (UT), were grown on 6-well-plates with a density of 20k per 1cm² until 13-15 DIV. All
 240 following steps were performed at 4°C. Neurons were kept on ice and washed twice with cold PBS.
 241 Subsequently, cells were detached by mechanical force. For total lysates, isolated cells were
 242 centrifuged at 4000rpm for 10 min, resuspended in 100µl lysis buffer (50mM Tris pH 7.9, 150mM
 243 NaCl, 5mM EDTA, 1% Triton X-100, 1% NP-40, 0.5% Deoxycholate, protease inhibitor cOmplete
 244 Tablets 1x) and incubated for 5 min on ice. Afterwards, cell suspension was centrifuged at 13000rpm
 245 for 10 min after which the supernatant was transferred into a new tube. For synaptosome suspension
 246 (and cytosol fraction) preparation, cortical or hippocampal neurons (both prepared according to
 247 *Preparation of cultured hippocampal neurons*) were treated with 2µM rapamycin for either 10 minutes
 248 or 2 hours. Next, cells were lysed in Syn-PER Synaptic Protein Extraction Reagent (Thermo Fisher
 249 Scientific, Waltham, USA) according to the manufacturers instructions. Briefly, cells were washed with
 250 cold PBS, detached by mechanical force in 100-200µl Syn-PER Reagent and centrifuged at 1200g for
 251 15 min. The supernatant was centrifuged at 15000g for 20 min and the cytosol fraction was collected.

252 Last, the synaptosome pellet was resuspended in Syn-PER Reagent. Subsequently, the protein
 253 concentration was determined using the Pierce BCA Protein Assay Kit (Thermo Fisher Scientific,
 254 Waltham, USA). The same amount of total protein (6.5-10µg) was then separated by SDS-PAGE and
 255 transferred onto a PVDF membrane. Afterwards, the membrane was blocked in 5% milk in TBS-T
 256 (20mM Tris, 150mM NaCl, 0.1% Tween-20) for 1 hour followed by primary antibody incubation
 257 (1:1000 in 3% milk in TBS-T) over night or for 72 hours at 4°C. The following antibodies were used:
 258 primary antibody against mCherry (1:1000; rabbit; Abcam, Cambridge, UK; Cat# ab167453), Actin
 259 (RRID: AB_476693) (1:1000; rabbit; Sigma-Aldrich, St. Louis, USA; Cat# A2066), Synaptophysin1
 260 (1:1000; mouse; Synaptic Systems, Göttingen, Germany; Cat# 101011) and LC3 (1:1000; rabbit;
 261 Sigma-Aldrich, St. Louis, USA; Cat# L7543). Afterwards, the membrane was washed three times with
 262 TBS-T for 10 min each and incubated with HRP-conjugated secondary antibody (1:2500 in 3% milk in
 263 TBS-T) (RRID: AB_772206, RRID: AB_772193) (Sigma-Aldrich, St. Louis, USA) for 1 hour at RT.
 264 Afterwards, the membrane was washed three times with TBS-T and bands were visualized using the
 265 imaging system Fusion FX7 (Vilber, Collégien, France) using 20x LumiGLO Reagent and 20x
 266 Peroxidase (Cell Signaling, Danvers, USA).

267
 268 *Photobleaching primary hippocampal neurons expressing Supernova/mCherry-constructs:* Primary
 269 hippocampal neurons grown in µ-Slide 8 Well Grid-500 ibiTreat (ibidi GmbH, Martinsried, Germany)
 270 culture dishes expressing Syp-Supernova, Syp-mCherry, Syp-lumSN, Syn-Supernova or Syp-Supernova
 271 cassettes were imaged at 13-15 DIV in Neurobasal Medium without phenol red (Thermo Fisher
 272 Scientific, Waltham, USA) at 37°C. Afterwards, a smaller diaphragm restricted area within the field of
 273 view was bleached for 60 seconds using 563nm wavelength light from a mercury lamp (100% HXP
 274 120 V, 43 HE filter set 563/581). Immediately after bleaching, a second image was taken confirming
 275 the radius of the bleached area. Subsequently, neurons were fixed at different time points (2-10 min,
 276 56-64 min, 116-124 min) after bleaching Supernova and immunostained with antibodies against
 277 Supernova (using a Killerred antibody), mCherry, GFP, Bassoon, Synaptotagmin1, Synaptophysin1,
 278 LC3 or Chmp2b (for procedure see *Immunocytochemistry of hippocampal neurons*). To scavenge ROS,
 279 60µM N-acetyl-L-cysteine (NAC) (in DMEM, Sigma-Aldrich, St. Louis, USA) was added right before the

280 bleaching and kept on the cells until fixation. For autophagy inhibition, 1 μ M wortmannin was added
 281 right before the bleaching and kept on the cells till fixation. After immunostaining, the same fields of
 282 view including the bleached areas were imaged utilizing the grid on the μ -Slide 8 Well Grid-500
 283 culture dishes.

284

285 *Basal autophagy in primary hippocampal neurons:* Primary hippocampal neurons in μ -Slide 8 Well
 286 Grid-500 ibiTreat (ibidi GmbH, Martinsried, Germany) culture dishes expressing FU-eGFP-LC3 were
 287 left untreated and fixed at 13-15 DIV. Afterwards, neurons were immunostained with antibodies
 288 against GFP, Bassoon and Synaptophysin1, Synapsin1 or Synaptotagmin1 (for procedure see
 289 *Immunocytochemistry of hippocampal neurons*).

290

291 *Electron microscopy:* Cultured hippocampal neurons were plated on astrocytes on carbon coated, 6mm
 292 sapphire disks at a density of 20k per 1cm² and infected with FU-Syp-Supernova-P2A-eGFP-LC3 at 2-3
 293 DIV. To better correlate regions of interest at the fluorescence and electron microscopy level, carbon
 294 was coated in the shape of an alphabetical grid on sapphire disks with the help of a metal mask (finder
 295 grid, Plano GmbH, Wetzlar, Germany). After a total of 13-15 days in culture, the sapphire disks were
 296 transferred into uncoated μ -Slide 8 Well to perform the bleaching experiment (for procedure see
 297 bleaching of primary hippocampal neurons expressing Supernova-constructs). Cryo-fixation using a
 298 high pressure freezing machine (EM-ICE, Leica, Wetzlar, Germany) was conducted at different time
 299 points after bleaching (10 min, 40 min) in Neurobasal medium without phenol red with the addition of
 300 a drop of 10% Ficoll solution (Sigma-Aldrich, St. Louis, USA) to prevent ice crystal damage. After
 301 freezing, samples were cryo-substituted in anhydrous acetone containing 1% glutaraldehyde, 1%
 302 osmium tetroxide and 1% milliQ water in an automated freeze-substitution device (AFS2, Leica). The
 303 temperature was kept for 4 hours at -90°C, brought to -20°C (5°C/h), kept for 12 hours at -20°C and
 304 then brought from -20°C to +20°C (5°C/h). Once at room temperature, samples were *en-bloc* stained in
 305 0.1% uranyl acetate in acetone, infiltrated in increasing concentration of Epoxy resin (Epon 812, EMS
 306 Adhesives, Delaware, USA) in acetone and finally embedded in pure Epon for 48 hours at 65°C.
 307 Sapphire disks were removed from the cured resin block by thermal shock. At this point the

308 alphabetical grid was visible on the resin block and was used to find back the bleached regions. The
 309 corresponding areas were excised from the block for ultrathin sectioning. For each sapphire, as a
 310 control, an additional resin blocks was excised from the quadrant opposite to the bleached area. 50nm
 311 thick sections were obtained using an Ultracut ultramicrotome (UCT, Leica) equipped with a Ultra 45
 312 diamond knife (Ultra 45, DiATOME, Hatfield, USA) and collected on formvar-coated 200-mesh copper
 313 grids (EMS). Sections were counterstained with uranyl acetate and lead citrate and imaged in a FEI
 314 Tecnai G20 Transmission Electron Microscope (FEI, Hillsboro, USA) operated at 80-200 keV and
 315 equipped with a Veleta 2K x 2K CCD camera (Olympus, Hamburg, Germany). Around 200 electron
 316 micrographs were collected (pixel size = 0.7nm) for each sample. Data were analyzed blindly using the
 317 ImageJ software. Double-membraned structures per presynaptic terminal were counted.

318
 319 *Electrophysiology:* Whole cell patch-clamp recordings were performed on autaptic hippocampal
 320 neurons at 13–18 DIV. All recordings were obtained at ~25°C from neurons clamped at –70 mV with a
 321 Multiclamp 700B amplifier (Molecular Devices, Sunnyvale, USA) under the control of Clampex 10.4
 322 software (Molecular Devices). Data were sampled at 10kHz and low-pass Bessel filtered at 3kHz.
 323 Series resistance was compensated at 70% and cells whose series resistance changed more than 25%
 324 throughout the recording session were excluded from the analysis. Neurons were immersed in
 325 standard extracellular solution consisting of 140mM NaCl, 2.4mM KCl, 10mM HEPES, 10mM glucose,
 326 2mM CaCl₂ and 4mM MgCl₂. The borosilicate glass electrodes (3-8 MΩ) were filled with the internal
 327 solution containing 136mM KCl, 17.8mM HEPES, 1mM EGTA, 0.6mM MgCl₂, 4mM ATP-Mg, 0.3mM
 328 GTP-Na, 12mM phosphocreatine, and 50U/ml phosphocreatine kinase. All solutions were adjusted to
 329 pH 7.4 and osmolarity of ~300mOsm. Coverslips with cultured neurons were placed on Olympus IX73
 330 microscope (Olympus, Hamburg, Germany) with 20x phase contrast objective. For Supernova
 331 bleaching, illumination from a Mercury Vapor Short Arc lamp (X-Cite 120PC Q, Excelitas Technologies,
 332 Waltham, USA) was filtered through a 560/40nm filter cube (Olympus U-FF mCherry) and controlled
 333 with a mechanical shutter. Lamp iris settings (100%) resulted in 71% bleaching of Supernova
 334 intensity (as compared to 22% of mCherry bleaching), after 60 seconds of illumination. From each
 335 neuron, 6 sweeps of EPSCs were evoked with a 2ms voltage step from -70mV to 0mV at 0.2Hz. Sixty

seconds illumination started immediately after end of 6th sweep, and after 5 min of waiting a second set of EPSCs was recorded. Control condition without illumination included a 6 min waiting period. During recordings with wortmannin, 1 μ M wortmannin solution was applied onto the cell using a fast-flow system from the beginning of first EPSC until end of recording session. Electrophysiological data were analyzed offline using Axograph X (RRID: SCR_014284) (Axograph Scientific, Berkeley, USA), Excel (Microsoft, Redmond, USA) and GraphPad Prism (GraphPad, La Jolla, USA).

Image acquisition and quantification: All images were acquired on a spinning disc confocal microscope (Zeiss Axio Observer.Z1 with Andor spinning disc and cobolt, omnicron, i-beam laser) (Zeiss, Oberkochen, Germany) (Andor, Belfast, UK) using either a 40x or 63x 1.4 NA Plan-Apochromat oil objective and an iXon ultra (Andor) camera controlled by iQ software (RRID: SCR_014461) (Andor). Images were processed using ImageJ (RRID: SCR_003070) and OpenView software (written by Dr. Noam Ziv, Technion Institute, Haifa, Israel). In brief with the OpenView software, multi-channel intensities were measured using a box routine associated with individual boutons. Boxes varied between 7x7 and 9x9 pixel in size, whereas settings were kept the same (e.g. thresholds). The average intensity (synaptic proteins, eGFP-LC3 et cetera) was calculated from all picked puncta and normalized to the control (untreated or unbleached). For quantification of # of puncta, separated axons were randomly picked and the number of puncta per unit length was counted manually. For Supernova experiments, axons were selected showing no or little eGFP-LC3 staining before bleaching. All Supernova evaluations were normalized to the unbleached control. To analyze the decrease in DHE_{blue} intensity following bleaching, HEK293 cells were marked in ImageJ using the Polygon selection tool and mean intensities of the identified areas were measured. Intensities of numerous samples were averaged and plotted. Band intensities of Western Blots were analyzed with the help of ImageJ and the Analyze>Gels tool. To determine the fraction of extrasynaptic eGFP-LC3 puncta positive for Syp-SN/Syn-SN/Syt-SN/Syp-lumSN/Synaptophysin1/Synapsin1/Synaptotagmin1, multi-channel images were manually scanned for eGFP-LC3 puncta within the bleached area that were not colocalizing with Bassoon. Out of these extrasynaptic eGFP-LC3 puncta, the fraction of eGFP-LC3 puncta positive for a specific synaptic protein was quantified. The fraction of extrasynaptic Syp-

364 SN/Syn-SN/Syt-SN/Syp-lumSN puncta positive for eGFP-LC3 was determined accordingly. For each
365 analysis, the following procedure was done: each experiment was performed with 2-4 independently
366 prepared cultures. During each Rapamycin experiment 1-2 coverslips were used. A total of 10 images
367 were taken from a maximum of 2 coverslips. From these, numerous synapses and up to 40 axons were
368 used for the analyses. For Supernova experiments, 2-4 independently prepared cultures were
369 bleached. During each experiment 2 wells for each time point were used. 1-2 images were taken per
370 time point per well leading to a total of approx. 20-30 axons and 60-250 synapses/puncta analyzed.
371 Depicted normalized means of intensities in puncta represent the means of all analyzed
372 synapses/puncta per experimental condition normalized to their in-culture controls.

373

374 *Experimental Design and Statistical Analyses:* Statistical design for all experiments can be found in the
375 figure legends. Independent experiments equal independent cultures. All data representations and
376 statistical analyses were performed with GraphPad Prism (RRID: SCR_002798).

377

378 Results

379 Monitoring presynaptic autophagy.

380 The primary goal of this study is to examine how and whether the local generation of ROS around
 381 SVs triggers a synaptic clearance response that removes damaged proteins. Based on previous studies
 382 showing that elevated ROS levels around organelles such as mitochondria lead to the activation of
 383 autophagy (Ashrafi et al., 2014; Wang et al., 2012; Yang and Yang, 2011), we anticipated that a similar
 384 generation of ROS around SVs may also induce a presynaptic autophagy based clearance program.
 385 Thus, while other clearance mechanisms, such as the endo-lysosomal or the proteasome system, could
 386 also be activated (see below), we initially sought to develop a live cell imaging based system that could
 387 detect changes in presynaptic autophagy, following different insults.

388 To achieve this goal, we initially created a lentiviral vector (FU-Syp-mCh-P2A-eGFP-LC3) that co-
 389 expresses mCherry-tagged Synaptophysin (Syp-mCh), as a presynaptic marker, and eGFP-tagged LC3,
 390 to detect autophagic vacuoles (AVs) (Figure 1A). To allow for the independent expression of Syp-mCh
 391 and eGFP-LC3, a P2A cleavage site was placed between the two coding sequences (Figure 1A). P2A is a
 392 highly efficient “self-cleaving” small peptide derived from porcine teschovirus-1 leading to
 393 posttranslational cleavage of the initially transcribed fusion protein (Kim et al., 2011). The vector was
 394 tested in a number of different assays. First, it was lentivirally transduced into Hela cells, where Syp-
 395 mCh and eGFP-LC3 both exhibited a largely diffuse cytoplasmic distribution (Figure 1B). The addition
 396 of 100μM chloroquine that impedes autophagic flux blocking lysosomal degradation (Galluzzi et al.,
 397 2016; Klionsky et al., 2012; Mauthe et al., 2018), resulted in a redistribution of eGFP-LC3 into a
 398 punctate pattern that colocalizes with total LC3 (endo- and exogenously expressed) and the
 399 autophagophore marker p62 (Johansen, 2011) (Figure 1B). However, Syp-mCh retained its diffuse
 400 cytosolic pattern and was not recruited into AVs (Figure 1B). These data indicate not only that the P2A
 401 site is efficiently cleaved, but also that eGFP-LC3 reliably reports the formation of AVs as previously
 402 reported (Klionsky et al., 2012; Mizushima et al., 2010; Okerlund et al., 2017).

403 In a second set of experiments, we examined whether Syp-mCh faithfully labeled presynaptic
 404 sites. Here, dissociated cultures of hippocampal neurons were infected to 30% with our lentiviral
 405 vector (FU-Syp-mCherry-P2A-eGFP-LC3) at 2-3 days *in vitro* (DIV) and analyzed by

immunocytochemistry at 13-15 DIV. Immunostaining of fixed cultures with antibodies to the postsynaptic density (PSD) protein Homer1 revealed that Syp-mCh forms puncta along the cell somas and dendrites of uninfected cells that colocalize with Homer1 puncta (Figure 1D), consistent with the presynaptic localization of other XFP-tagged Synaptophysin as reported previously (Li et al., 2010). A comparison of Syp-mCh and eGFP-LC3 signals in primary hippocampal neurons during live cell imaging reveals that a small fraction (~10%) of the Syp-mCh positive puncta colocalizes with eGFP-LC3 positive puncta (Figure 1C). The minimal colocalization suggests that the P2A site is functioning properly to uncouple these two proteins. This concept is further supported by Western Blots of cellular lysates of infected hippocampal neurons stained with a mCherry antibody. Here, greater than 95% of the immunoreactivity is present in the 70kDa Syp-mCh band versus the uncleaved 120kDa Syp-mCh-P2A-eGFP-LC3 band (Figure 1E), supporting the conclusion that once expressed in neurons each reporter is free to operate independently.

In a third set of experiments, we examined how the induction of autophagy with 2 μ M of the mTOR inhibitor rapamycin (Boland et al., 2008; Hernandez et al., 2012; Spilman et al., 2010) affected the distribution of eGFP-LC3 relative to Syp-mCh in neurons. Initially, rapamycin was added to sparsely FU-Syp-mCherry-P2A-eGFP-LC3 expressing hippocampal cultures (13-15 DIV) for 2 hours, as most previous studies had shown that this condition can induce autophagy in neurons (Hernandez et al., 2012). To identify 'synaptic' changes in eGFP-LC3 levels, we analyzed the average intensities of eGFP-LC3 puncta that colocalized with Syp-mCh puncta in fixed neurons. This revealed a modest (36%) but significant increase in eGFP-LC3 intensities within presynaptic boutons compared to untreated control neurons (Figure 1F and I). Monitoring the number of eGFP-LC3 puncta per unit length of axon revealed that 2 hours of rapamycin treatment significantly increased the number of eGFP-LC3 puncta present in axons compared to non-treated control neurons (Figure 1F and J). These data are consistent with the concept that rapamycin can induce the formation of autophagosomes/AVs in hippocampal axons. However, given that vesicular transport is quite rapid, it is unclear whether during the 2-hour period the newly formed AVs arose at synapses and dispersed into the axons and/or were generated within axons and then accumulate within presynaptic boutons. We thus explored whether AVs would appear in as little as 10 minutes following the addition of rapamycin. Surprisingly, we found that not

only did eGFP-LC3 puncta appear in axons during this short period of induction (Figure 1G and L), but eGFP-LC3 intensity was dramatically increased within presynaptic boutons marked with Syp-mCh (Figure 1G and K). Importantly, we also found that appearing eGFP-LC3 puncta were positive for the autophagy cargo receptor p62 (Johansen, 2011) (Figure 1H and M), suggesting that they are indeed autophagosomes and are forming locally within presynaptic boutons. To further explore whether the observed rapamycin-induced AV formation at synapses is induced via the canonical autophagy pathway, which includes the PI3K Vps34 (Lilienbaum, 2013; Rubinsztein et al., 2012), we included 1 μ M wortmannin, a general PI3K inhibitor (Carpenter and Cantley, 1996; Klionsky et al., 2012), together with rapamycin during the 10 minutes incubation period. This manipulation abolished the accumulation of eGFP-LC3 puncta in both presynaptic boutons (marked with Syp-mCh) (Figure 1N and O) and along axons (Figure 1N and P). Taken together these data indicate that the machinery necessary for the rapid generation of AVs is located within or very near to presynaptic boutons and can be triggered by a PI3K-dependent pathway.

To corroborate the novel finding that rapamycin induces synaptic autophagy within 10 minutes (Figure 1K), cortical and hippocampal neurons were treated with 2 μ M rapamycin for either 10 minutes or 2 hours and subsequently lysed and prepared for Western Blot analyses. In order to quantify predominantly synaptic autophagy, synaptosomes (synaptosome suspension) were enriched leading to a strong Synaptophysin signal compared to the cytosol fraction (Figure 2A). The soluble form of LC3 is defined as LC3-I, LC3 that is conjugated to the autophagosome is defined as LC3-II. Thus, LC3-II is an excellent marker to monitor autophagy (Fleming et al., 2011; Mizushima et al., 2010; Satoo et al., 2009). In our Western Blot experiments, both LC3-I and LC3-II bands were increased after 10 minutes of rapamycin treatment in cortical (Figure 2A and C) and hippocampal neurons (Figure 2B and E) compared to untreated control cells. However, the increase in LC3-II is higher in hippocampal neurons than in cortical neurons indicating that hippocampal neurons are more sensitive to rapamycin-dependent autophagy induction. After a 2-hour treatment of rapamycin, LC3-I and LC3-II levels are still elevated in both cortical (Figure 2A and D) as well as hippocampal (data not shown) neurons. Together, these observations support our conclusion that synaptic autophagy can be induced by rapamycin treatment within a short minute time frame.

462

463 **Light-activated ROS generation triggers presynaptic autophagy.**

464 The ability of rapamycin to induce presynaptic autophagy within 10 minutes strongly suggests
 465 that presynaptic boutons contain local clearance mechanisms, such as autophagy, that could in
 466 principle deal with locally damaged proteins in real-time. As a direct test of this hypothesis, we
 467 explored whether the real-time damage of SV proteins via the production of reactive oxygen species
 468 (ROS) (Takemoto et al., 2013) could also trigger the rapid clearance of these molecules via, e.g.
 469 autophagy. To accomplish this goal, we made use of a molecular variant of GFP called Supernova, a
 470 monomeric version of KillerRed (Bulina et al., 2006), previously shown to generate ROS following its
 471 excitation with 550-590nm light (Takemoto et al., 2013). As other photosensitizers, short-lived ROS
 472 generated by Supernova are expected to damage proteins within 1-4nm of the source (Linden et al.,
 473 1992; Takemoto et al., 2013). Thus to restrict the actions of the ROS to SVs, we initially fused
 474 Supernova to the short cytoplasmic tail of the SV protein Synaptophysin (creating Synaptophysin-
 475 Supernova; Syp-SN). This was then subcloned and co-expressed with eGFP-LC3 via our lentiviral
 476 vector (FU-Syp-Supernova-P2A-eGFP-LC3) (Figure 3A) (see also Figure 9A).

477 As with the FU-Syp-mCherry-P2A-eGFP-LC3 vector, we then verified that both the Syp-SN and
 478 eGFP-LC3 portions of the vector were expressed and processed. We also verified that the eGFP-LC3
 479 segment was recruited to p62 positive AVs in HeLa cells treated with chloroquine and that Syp-SN
 480 properly localized at Homer1 positive synapses as Syp-mCh (data not shown). Moreover, we
 481 confirmed in HeLa cells that 80% of the Supernova fluorescence could be photobleached during a 60
 482 seconds exposure of 563nm wavelength light from a mercury lamp.

483 To explore whether bleaching of Syp-SN can induce presynaptic autophagy, primary hippocampal
 484 neurons grown on μ -Slide 8 Well culture dishes were sparsely infected with FU-Syp-Supernova-P2A-
 485 eGFP-LC3 lentivirus at 2-3 DIV. Around 14 DIV, they were transferred to a spinning disc confocal
 486 microscope equipped with a temperature controlled live cell imaging chamber. Prior to bleaching
 487 selected fields of view, axons from infected neurons growing on top of uninfected neurons were
 488 selected and imaged during excitation with a 491nm (for the eGFP-LC3 signal) and a 561nm laser (for
 489 the Syp-SN signal). Subsequently, a subregion, selected with a field diaphragm, was bleached by

490 exposing cells to 563nm light from a mercury lamp for 60 seconds (Figure 3B), a condition found to
 491 bleach approximately 80% of the initial fluorescence. Cultures were fixed 5-120 minutes post
 492 bleaching and immunostained with antibodies against GFP and Supernova, allowing the post-hoc
 493 identification of synapses within and outside of the bleached area and the levels and redistribution of
 494 eGFP-LC3. Comparing the intensity of eGFP-LC3 at Syp-SN positive puncta within and outside the
 495 bleached area revealed a significant increase in synaptic eGFP-LC3 intensity in the bleached area
 496 within 5 minutes of initial bleaching (Figure 3C and F). However, at that time point, the number of
 497 eGFP-LC3 puncta per axon unit length is not changed compared to the unbleached control (Figure 3C
 498 and G). Similarly, 1 hour after bleaching, eGFP-LC3 levels are still elevated in Syp-SN positive synapses
 499 inside the bleached area compared to outside, with only a modest increase in the number of eGFP-LC3
 500 puncta per unit length of axon (Figure 3D, H and I). Intriguingly, 2 hours after triggering ROS
 501 production, eGFP-LC3 levels remain somewhat elevated at Syp-SN positive synapses, and dramatically
 502 accumulated as small puncta along axons inside the bleached area (Figure 3E, J and K) compared to
 503 those outside. These latter data imply that the synaptic increase in ROS rapidly induces presynaptic
 504 autophagy and that subsequent flux carries the autophagosomal membranes into axons.

505 Although bleaching of Supernova is described to coincide with ROS generation (Jarvela and
 506 Linstedt, 2014), we additionally made use of the superoxide indicator dihydroethidium (DHE) to
 507 monitor for ROS production (Figure 4A and B). DHE exhibits blue light in the cytoplasm. In the
 508 presence of superoxides, DHE intercalates with the DNA and emits red light from the nucleus. This
 509 redistribution causes the blue fluorescence in the cytoplasm to drop upon ROS production, which is
 510 used as a measure of superoxide generation. Bleaching FU-Syp-Supernova-P2A-eGFP-LC3 transfected
 511 HEK293 cells incubated with DHE shows a significantly higher decrease in DHE_{blue} intensity compared
 512 to bleaching FU-Syp-mCherry-P2A-eGFP-LC3 transfected and untransfected (UT) control cells (Figure
 513 4A and B) confirming superoxide generation after Supernova bleaching, as previously shown
 514 (Takemoto et al., 2013). Note that DHE_{blue} intensity also decreases in the presence of FU-Syp-mCherry-
 515 P2A-eGFP-LC3 compared to UT control cells indicating that already bleaching mCherry leads to the
 516 production of ROS, however not as efficient as Supernova (Figure 4B). Thus, we further investigated
 517 the capability of mCherry bleaching mediated ROS production to induce synaptic autophagy.

518 Intriguingly, Syp-mCh puncta show increased eGFP-LC3 levels compared to unbleached control
 519 boutons 1 hour after bleaching (Figure 4C). However, eGFP-LC3 levels after Syp-SN bleaching are
 520 significantly higher than after Syp-mCh bleaching (Figure 4C, D and F). Furthermore, 60 μ M of the ROS
 521 scavenger N-acetyl-L-cysteine (NAC), added to FU-Syp-Supernova-P2A-eGFP-LC3 infected cells before
 522 bleaching, diminishes, although not statistically significant, the earlier observed increase in eGFP-LC3
 523 intensities at synapses (Figure 4D, E and F). These data indicate that Supernova is a potent ROS
 524 generator and that the rapid induction of synaptic autophagy is caused by a light-activated local
 525 increase of ROS near SVs.

526 To rule out that increased eGFP-LC3 levels after Syp-SN bleaching are simply caused by the slight
 527 overexpression of LC3 (eGFP-LC3), we also measured endogenous LC3 levels after bleaching in
 528 neurons only expressing FU-Syp-Supernova (Figure 5A). In accordance with our previous findings
 529 (Figure 3), Syp-SN bleaching leads to a rapid increase in endogenous LC3 intensities at presynaptic
 530 boutons identified through the presence of Bassoon within minutes (Figure 5B and E) and LC3 levels
 531 remain elevated for additional 2 hours (Figure 5C, D, F, G). Both data with endogenous LC3 as well as
 532 eGFP-LC3 confirm that local light-activated ROS production can induce synaptic autophagy within a
 533 short time period as quick as 5 minutes. This is in line with our observation that rapamycin can induce
 534 autophagy within 10 minutes (Figure 1).

535

536 **ROS-induced synaptic autophagy is PI3K- and Atg5-dependent.**

537 To investigate whether the observed ROS-induced elevation of eGFP-LC3 is dependent on the
 538 canonical PI3K/Vps34 autophagy pathway, 1 μ M wortmannin was added to neurons before bleaching
 539 Syp-SN and maintained in the culture for the following 2 hours, after which neurons were fixed and
 540 analyzed. In cells that were not treated with wortmannin, eGFP-LC3 intensity within presynaptic
 541 boutons as well as the number of eGFP-LC3 puncta per unit length of axon remained elevated (Figure
 542 6A, C and D) compared to the unbleached control. In contrast, the inclusion of wortmannin was found
 543 to inhibit the light-activated increase in eGFP-LC3 intensity within presynaptic boutons (Figure 6B and
 544 E), but had no effect on the number of eGFP-LC3 puncta per unit length of axon (Figure 6B and F).
 545 These data indicate that the ROS-induced increase in presynaptic autophagy may be dependent on the

PI3K signaling pathway, while autophagy within axons is not. Note that while most of the Syp-SN is synaptic (data not shown), extrasynaptic pools are likely present, presumably engaged in the active transport within mobile pools of SVs (Cohen et al., 2013; Maas et al., 2012; Tsurriel et al., 2006). Photobleaching damage of this pool could thus contribute to a PI3K-independent form of axonal autophagy in axons, as already described for other cell types (Chu et al., 2007; Lemasters, 2014; Zhu et al., 2007).

Additionally, given the caveat that wortmannin is not a selective inhibitor for Vps34 (Bain et al., 2007), we made use of a knock down approach using an shRNA against the autophagy-related protein Atg5 (shAtg5) to inhibit autophagy. To ensure co-expression of Syp-SN, eGFP-LC3 and the shRNA, an U6 promoter and the small hairpin RNA were integrated upstream into the vector FU-Syp-Supernova-P2A-eGFP-LC3 (F-U6-shAtg5-U-Syp-Supernova-P2A-eGFP-LC3). A scrambled shRNA (scRNA/SC) served as a control (F-U6-scRNA(SC)-U-Syp-Supernova-P2A-eGFP-LC3). Strikingly, neurons expressing the scRNA depict increased eGFP-LC3 levels at Syp-SN puncta as well as an increased number of eGFP-LC3 puncta along axon segments 2 hours after bleaching (Figure 6G, I and J), thus resembling earlier outcomes (Figure 6A, C and D). However, when shAtg5 is additionally expressed in neurons, its presence inhibits the light-activated increase of synaptic eGFP-LC3 and the number of eGFP-LC3 puncta (Figure 6H, K and L). These data confirm that ROS-induced eGFP-LC3 accumulation is dependent on canonical autophagy initiation.

ROS-induced damage to Synaptophysin promotes AV formation.

The appearance of eGFP-LC3 positive puncta within the axons and presynaptic boutons of Synaptophysin-Supernova expressing cells following photobleaching suggests that this insult induces the autophagic clearance of damaged SVs and their proteins. To formally test this hypothesis, we performed transmission electron microscopy of FU-Syp-Supernova-P2A-eGFP-LC3 expressing hippocampal neurons. Infected neurons grown on sapphire disks were photobleached with 563nm light from a mercury lamp for 60 seconds. Similar to our live imaging experiments, a field diaphragm was used to create bleached and unbleached regions on the same sapphire disk before high pressure freezing and further processing for EM. The number of double-membraned organelles (autophagic

574 vacuoles = AVs) within presynaptic boutons or SVs containing axonal varicosities were then quantified
 575 as performed previously (Okerlund et al., 2017) (Figure 7A). Consistent with our light level studies
 576 (Figure 3F), significantly more AVs per presynaptic terminal were observed 10 minutes after light-
 577 activated Synaptophysin damage within the bleached area compared to the unbleached area (Figure
 578 7C and D). Images analyzed ~40 minutes after bleaching revealed a slight but non-significant increase
 579 in AVs/terminal (Figure 7F and G). These data indicate that most newly formed autophagosomes leave
 580 the synapse.

581 Conceptually, local ROS-induced damage of synaptic proteins could induce not only autophagy but
 582 also other degradative pathways such as the endo-lysosomal system. One hallmark of the endo-
 583 lysosomal system is the appearance of multivesicular bodies (MVBs) (Ceccarelli et al., 1973; Raiborg
 584 and Stenmark, 2009). We thus examined whether the light-activated damage of Synaptophysin also
 585 induces the endo-lysosomal pathway by quantifying the presence of synaptic MVBs within
 586 photobleached presynaptic boutons by EM (Figure 7B). Intriguingly, no change in their number was
 587 observed at either 10 or 40 minutes after photobleaching compared to unbleached boutons (Figure 7E
 588 and H), indicating that the ROS-mediated damage of Synaptophysin primarily triggers the activation of
 589 autophagy. To confirm this observation, we also monitored whether markers of the endo-lysosomal
 590 pathway accumulated in presynaptic boutons following light-activated damage of Synaptophysin.
 591 Strikingly, level of the late endosome marker Rab7 are increased at presynaptic boutons 5 minutes
 592 after bleaching (Figure 8B and E), and stay elevated compared to the unbleached control for at least 2
 593 more hours (Figure 8E, G and I). Since Rab7 is also abundant on autophagosomes, we stained for
 594 another, more specific, MVB marker Chmp2b, which is part of the ESCRT-III complex (Vingtdeux et al.,
 595 2012). Interestingly, Chmp2b also accumulates at boutons 1 hour after bleaching (Figure 8C and H).
 596 These observations indicate that ROS-mediated damage to Synaptophysin/SVs may also engage other
 597 degradative pathways such as the endo-lysosomal system.

598

599 **ROS-induced damage to several presynaptic proteins induces presynaptic autophagy.**

600 As ROS generated by illuminating Supernova is anticipated to damage proteins only within 1-4nm
 601 of the sources (Jacobson et al., 2008; Takemoto et al., 2013), it seems reasonable to predict that the

induction of presynaptic autophagy is linked to the damage of proteins, which are then sorted and gathered into the interior of the newly forming autophagophore membrane. If true, the damage to other presynaptic proteins should also lead to the induction of autophagy (Figure 9A).

To test this hypothesis, we coupled Supernova to two additional SV proteins, Synaptotagmin (Syt), an integral membrane protein with a long cytoplasmic tail (Chapman, 2002; Hilfiker et al., 1999), and Synapsin (Syn), a larger cytosolic protein (Figure 9A) that dynamically associates with the outer surface of SVs in an activity-dependent manner (Chi et al., 2001; Waites and Garner, 2011). To permit the simultaneous detection of presynaptic autophagy, we co-expressed Syt-SN or Syn-SN with eGFP-LC3 via our lentiviral vector (FU-Syt-SN-P2A-eGFP-LC3; FU-Syn-SN-P2A-eGFP-LC3). In control experiments, we confirmed that both Syt-SN and Syn-SN and eGFP-LC3 were appropriately processed and that Syt-SN and Syn-SN retained their ability to become selectively localized to presynaptic boutons (data not shown). As described above for Syp-SN, neurons infected at 2-3 DIV were bleached at 13-15 DIV for 60 seconds and the intensity of eGFP-LC3 within presynaptic boutons quantified. Interestingly, eGFP-LC3 intensity in Syt-SN and Syn-SN puncta as well as the number of eGFP-LC3 puncta along axons did not change within 5 minutes of photobleaching (Figure 9B, E, H and K) compared to unbleached boutons. However, 1 hour after light-activated damage to either Synaptotagmin or Synapsin, eGFP-LC3 intensity significantly increased within presynaptic boutons immuno-positive for Syt-SN (Figure 9C and F) and Syn-SN (Figure 9I and L). When fixed 2 hours after ROS production, eGFP-LC3 levels remained slightly elevated at bleached Syn-SN positive synapses (Figure 9J and M), but returned to unbleached levels in Syt-SN positive synapses (Figure 9D and G). Taken together, these data indicate that, as Synaptophysin, the local ROS-mediated damage to Synaptotagmin and the SV-associated protein Synapsin can induce presynaptic autophagy, albeit at attenuated slower rates. These data indicate that the induction of presynaptic autophagy is tightly coupled to ROS damage to synaptic proteins, and thus associated with the normal clearance of misfolded or damaged proteins.

Supernova-tagged proteins are more abundant in ROS-induced autophagy organelles than endogenous SV proteins.

630 To date several studies have demonstrated that autophagosomes form in axons upon starvation,
 631 rapamycin treatment as well as enhanced synaptic activity (Maday and Holzbaur, 2014; Wang et al.,
 632 2015) and become retrogradely transported along the axon towards the soma (Cheng et al., 2015a;
 633 Maday et al., 2012). An unresolved question is which synaptic proteins become associated with
 634 autophagic cargos. A related question is whether presynaptic autophagy leads to the en-mass removal
 635 of SVs or whether it can selectively scavenge damaged proteins. Our ability to damage SV proteins
 636 with light and induce autophagy provides a unique opportunity to explore these questions. In an initial
 637 experiment, we examined whether Syp-SN appears in extrasynaptic eGFP-LC3 positive puncta
 638 following light-activated ROS production. To distinguish between synaptic and extrasynaptic eGFP-
 639 LC3 organelles, cultures were fixed and stained with antibodies against the presynaptic active zone
 640 protein Bassoon and quantified for the fraction of extrasynaptic eGFP-LC3 puncta negative for
 641 Bassoon but positive for synaptic proteins 1 hour after bleaching.

642 In experiments with Syp-SN, we observed that more than 70% of extrasynaptic eGFP-LC3 puncta
 643 (also referred to as autophagy cargo organelles) are positive for Syp-SN (Figure 10A and D). This
 644 suggests that ROS-damaged Syp-SN is indeed a cargo of these organelles. To investigate whether the
 645 presence of Syp-SN in autophagy cargo organelles represents the en-mass engulfment of SVs or the
 646 selective removal of this damaged protein, we monitored the distribution of endogenous
 647 Synaptotagmin1 (Syt1) within the same neurons, a second core constituent of SVs, in extrasynaptic
 648 autophagy organelles following light-induced damage to Syp-SN. As Synaptotagmin1 is not known to
 649 directly interact with Synaptophysin, we reasoned that the ROS-mediated damage to Syp-SN would
 650 not necessarily damage Synaptotagmin on the same SV. Interestingly, the fraction of extrasynaptic
 651 autophagy organelles that are positive for Synaptotagmin1 (Syt1) is dramatically smaller than the
 652 fraction of Syp-SN positive autophagy cargo organelles (Figure 10A and D).

653 To confirm the selectivity of autophagic cargo after Supernova-induced damage, we performed
 654 the experiment vice versa and quantified the fraction of Syt-SN positive extrasynaptic autophagy cargo
 655 organelles 1 hour after bleaching. As with Syp-SN, more than 65% of the extrasynaptic eGFP-LC3
 656 puncta colocalized with Syt-SN, while only 18% of the endogenous Synaptophysin1 (Syp1) was

657 present at these sites (Figure 10B and E). These data indicate that the autophagic machinery within
 658 presynaptic boutons can detect and selectively remove damaged SV proteins.

659 The selectivity of the autophagic cargo points towards a selective tagging of the damaged
 660 Supernova fusion protein. This tagging likely happens at the cytoplasmic side of the SVs as this is
 661 where the degradation machinery is located. To test this hypothesis, we fused Supernova to
 662 Synaptophysin between the third and fourth transmembrane domain resulting in a luminal Supernova
 663 (FU-Syp-lumSN-P2A-eGFP-LC3). Here, we did not observe an accumulation of eGFP-LC3 at bleached
 664 Syp-lumSN positive boutons (data not shown). Intriguingly, the fraction of Syp-lumSN positive
 665 extrasynaptic autophagy cargo organelles is very low (Figure 10C and F) compared to Syp-SN (Figure
 666 10D) indicating that bleached Syp-lumSN does not become cargo of autophagy organelles after ROS-
 667 induced autophagy.

668 The low but significant presence of endogenous Synaptophysin1 and Synaptotagmin1 in eGFP-
 669 LC3 puncta could arise either from the peripheral damage of ROS or be part of the basal flux of these
 670 proteins through this pathway. We thus examined whether under basal conditions endogenous
 671 Synaptophysin1 and Synaptotagmin1 versus Synapsin1 associate with extrasynaptic eGFP-LC3 puncta.
 672 Here, we observed that higher levels of both endogenous Synaptophysin1 and Synaptotagmin1 were
 673 found at extrasynaptic eGFP-LC3 puncta compared to Synapsin1 (Figure 10G and H). These data
 674 indicate that these former SV proteins may be cleared through this degradative pathway also under
 675 basal conditions. Additionally, these data indicate that autophagy plays a minor role in the clearance of
 676 Synapsin1.

677

678 **Synaptic autophagy acts as a beneficial surveillance mechanism maintaining synapse function.**

679 A fundamental question within the synaptic proteostasis field is what roles do different clearance
 680 systems play during synaptic transmission. Most studies to date on autophagy rely either on the
 681 analysis of genetic ablation and inactivation of key autophagic proteins (Atg5 and Atg7) (Rubinsztein
 682 et al., 2011; Russell et al., 2014) or the activation of autophagy with drugs like rapamycin, none of
 683 which are specific for the synapse and generally trigger a homeostatic response from other systems
 684 masking a specific role of autophagy in the system. Having shown that light-activated ROS production

685 can be used to rapidly (5 minutes) trigger the autophagic clearance of selectively damaged SV
686 proteins, we were keen to explore whether presynaptic autophagy contributes to the real-time
687 maintenance of synaptic function.

688 We therefore performed electrophysiological experiments. EPSC amplitudes were recorded from
689 autaptic neurons, infected with FU-Syp-SN-P2A-eGFP-LC3 lentivirus at 2-3 DIV, at 13-18 DIV.
690 Interestingly, bleaching alone did not robustly change the EPSC amplitude (Figure 11A and D) and
691 neither did treatment with 1 μ M wortmannin without bleaching (Figure 11B and D). However, under
692 autophagy inhibition with 1 μ M wortmannin light-activated ROS production leads to a significant
693 decrease in EPSC amplitudes (Figure 11C and D). A similar effect could be observed when autophagy
694 was inhibited by knocking down Atg5. Intriguingly, neurons expressing shRNA against Atg5 (shAtg5)
695 alone did not show an altered EPSC amplitude (Figure 11F and H) indicating that basal autophagy is
696 not necessary for synapse function. However, challenging the system through the light-activated ROS
697 production leads to a significant decrease of the EPSC amplitude in neurons expressing shAtg5 (Figure
698 11G and H) but not in neurons expressing scrambled shRNA (Figure 11E and H). Together these data
699 nicely support the hypothesis that autophagy can play a real-time role in the maintenance of synaptic
700 transmission helping the synaptic terminals to cope with protein damaging insults.

701 Discussion

702 Mechanisms regulating quality control and turnover of synaptic proteins are fundamental to
 703 synapse integrity, however, they are not well understood. In this study, we provide evidence that
 704 autophagy can be rapidly induced within presynaptic boutons either by rapamycin or by the selective
 705 damage of SV proteins through superoxides. The time range of autophagy induction is consistent with
 706 the concept that the machinery is maintained and regulated within presynaptic boutons. Our data also
 707 suggest a real-time role for autophagy in maintaining synaptic function, as without it the accumulation
 708 of damaged SV proteins can compromise synaptic transmission.

709 A prerequisite for a real-time functionality for autophagy within presynaptic boutons is its
 710 activation on short time scales after insults that damage presynaptic proteins. Studies show that
 711 autophagic organelles appear within axons and presynaptic boutons 3-7 hours following the addition
 712 of rapamycin (Hernandez et al., 2012) or 48 hours after treatment with Sonic Hedgehog (Petrulia et al.,
 713 2013). A high potassium stimulus also increased the appearance of LC3-positive puncta within tens of
 714 minutes in axons (Wang et al., 2015) and dendritic spines (Shehata et al., 2012) indicating that the
 715 autophagic machinery can be activated within different neuronal compartments. Mechanistically,
 716 Bassoon, as well as presynaptic proteins like Rab26 and Endophilin A have been functionally linked to
 717 autophagy (Binotti et al., 2015; Okerlund et al., 2017; Soukup et al., 2016; Vanhauwaert et al., 2017) of
 718 which Atg5, Atg16, LC3 and p62 have been localized to presynaptic boutons (Okerlund et al., 2017).
 719 However, as autophagosomes are highly mobile (Cheng et al., 2015b; Maday et al., 2012), it remains
 720 unclear whether they arise within boutons or simply accumulate there.

721 In the current study, we developed a lentiviral vector, expressing a SV protein and the autophagy
 722 marker LC3 to monitor autophagic structures in real-time. Similar to earlier studies (Hernandez et al.,
 723 2012), we observed low basal autophagy levels within axons (Figure 1F). However, eGFP-LC3 levels
 724 increase within 10 minutes within presynaptic boutons and axons following 2 μ M rapamycin treatment
 725 (Figure 1G, K and L). The rapid LC3 increase seen on the light microscopy level could also be seen in
 726 Western Blot analyses using synaptosomes (Figure 2E). Synaptic eGFP-LC3 accumulation appears to
 727 be due to elevated autophagy as its increase was blocked by 1 μ M wortmannin and Atg5 knock down
 728 (Figure 1N-P, Figure 6K and L) (Codogno et al., 2011; Mizushima et al., 2011).

729 Although the induction of presynaptic autophagy is faster than previously recognized, the
 730 addition of rapamycin is neither specific for any one neuronal compartment, nor a natural inducer of
 731 autophagy (Deng et al., 2017). Therefore we developed a vector system that allows us to generate a
 732 spatiotemporally controlled insult within presynaptic boutons. Here, we made use of the fact that free
 733 radicals trigger the damage of proteins *in vivo* (Jarvela and Linstedt, 2014) and tagged synaptic
 734 proteins with the genetically encoded photosensitizer Supernova (Takemoto et al., 2013). With similar
 735 approaches, it has been possible to acutely damage mitochondria and induce mitophagy (Ashrafi et al.,
 736 2014; Wang et al., 2012; Yang and Yang, 2011).

737 ROS-induced damage of Synaptophysin led to a rapid induction of autophagy, indicated by the
 738 accumulation of eGFP-LC3 within presynaptic boutons within 5 minutes and its spread into axons over
 739 time (1-2 hours) (Figure 3I and K). The fast temporal accumulation of LC3 in boutons was also
 740 observed for autophagic vacuoles, as detected by electron microscopy (Figure 7D). These data indicate
 741 that the autophagy machinery is present within presynaptic terminals and can be engaged following a
 742 local insult to SV proteins within minutes.

743 A fundamental question raised by our study is whether ROS damage to SV proteins exclusively
 744 turns on autophagy as the clearance mechanism or multiple protein degradation systems. The endo-
 745 lysosomal system has been reported to also clear SV proteins in response to ongoing synaptic activity
 746 (Sheehan et al., 2016; Uytterhoeven et al., 2011). One hallmark of this pathway is the appearance of
 747 multivesicular bodies (MVBs) (Raiborg and Stenmark, 2009). We failed to observe an increase in the
 748 number of synaptic MVBs on electron microscopy level (Figure 7E and H), indicating that in contrast to
 749 autophagy, the endo-lysosomal system is not robustly engaged by ROS-mediated protein damage.
 750 However, monitoring Rab7 and Chmp2b levels (Sheehan et al., 2016; Stenmark, 2009) by light
 751 microscopy, we did observe a modest increase in their colocalization with Synaptophysin-SN,
 752 following ROS production (Figure 8). Thus we cannot presently rule out that ROS-mediated damage to
 753 SV proteins can also trigger the activation of several degradative systems. Interestingly, Sheehan et al.
 754 (2016) show that only a subset of SV proteins are preferentially degraded by the endo-lysosomal
 755 system, highlighting the importance to address in the future if distinct SV proteins are degraded via
 756 specific and therefore separate pathways and how they are being tagged.

757 Our data indicate that autophagy induction is not solely dependent on the damage of
758 Synaptophysin, as the destruction of Synaptotagmin as well as Synapsin also leads to elevated
759 autophagy levels at presynapses (Figure 9). However, for Synaptotagmin-SN and Synapsin-SN eGFP-
760 LC3 levels increased with a slower time course (~1 hour) (Figure 9). The discrepancy could be due to
761 differences in what fraction of SV proteins are damaged by ROS, a situation that would be influenced
762 by the relative abundance of the Supernova-tagged proteins and/or the number of juxtaposed SV
763 proteins that are additionally damaged by ROS. Interestingly, Synaptophysin has the highest copy
764 number per SV compared to Synaptotagmin and Synapsin (Takamori et al., 2006). Future studies could
765 help resolve this issue and/or whether some SV proteins are more directly linked to the induction of
766 synaptic autophagy.

767 An additional question raised by our study is whether the clearance mechanisms triggered by
768 ROS-mediated damage lead to the selective removal of only the damaged SV protein or the elimination
769 of the entire SV. Indeed, about 70% of extrasynaptic eGFP-LC3 puncta were also positive for
770 Synaptophysin-SN following ROS-mediated damage (Figure 10D). Intriguingly, a much smaller fraction
771 (18%) of these puncta were also positive for endogenous SV protein Synaptotagmin, which does not
772 directly interact with Synaptophysin (Bonanomi et al., 2007; Rizzoli, 2014). These data suggest that
773 presynaptic autophagy can specifically remove damaged SV proteins from synapses. This concept is
774 supported by a reciprocal experiment performed with neurons expressing Synaptotagmin-SN. Here,
775 we also observed a dramatic recruitment of Synaptotagmin-SN into extrasynaptic eGFP-LC3 puncta,
776 but only modest levels of endogenous Synaptophysin (Figure 10E), implying that ROS-mediated
777 damage caused by Supernova is rather limited and primarily affects juxtaposed proteins, a concept
778 consistent with the low quantum yield of Supernova (Shu et al., 2011; Trewin et al., 2018) and the
779 limited damage half-radius of 3-4nm (Takemoto et al., 2013). Importantly, the inability of
780 photobleaching luminally localized Supernova to trigger the sorting of Syp-lumSN into autophagy
781 organelles (Figure 10F) indicates that ROS damage has to occur on the cytoplasm face of SV proteins to
782 be recognizable for the autophagic machinery. Conceptually, a selective removal model also makes
783 metabolic sense, as it would allow for the differential removal of specific mis-folded or damaged
784 proteins, consistent with different half-lives of SV proteins (Cohen et al., 2013). Although the

785 mechanism of selective removal remains unclear, we hypothesize that SV proteins are directly
786 removed from SVs or that their removal is dependent on an intermediary endosomal sorting step.
787 Further studies will be necessary to discriminate between these options.

788 The rapid induction of presynaptic autophagy within minutes suggests that autophagy possibly
789 has real-time functions at synapses, e.g. helping to maintain synaptic health and integrity. Studies by
790 Lin et al. (2013) showed that tagging Synaptophysin with miniSOG leads to a real-time disruption of
791 neurotransmitter release following light activation. In contrast, in our experiments with
792 Synaptophysin-SN, we did not observe an overt change in synaptic function, assessed by the evoked
793 release of neurotransmitter following light-activated ROS production (Figure 11). This suggests that
794 protein damage caused by Synaptophysin-Supernova radiation is less potent than that induced with
795 miniSOG-Synaptophysin. Intriguingly, when the induction of autophagy was blocked during ROS-
796 mediated damage of Synaptophysin-SN, the evoked EPSC amplitudes were reduced (Figure 11),
797 indicating that upon autophagy inhibition, damaged synaptic proteins accumulate within presynaptic
798 terminals having a direct impact on neurotransmitter release and thus EPSC amplitude. Conceptually,
799 the decrease in EPSC amplitude could also be explained by a postsynaptic effect, e.g. a down-regulation
800 of postsynaptic receptors. Given that Supernova is directly tethered to a SV protein, the most likely
801 effect of ROS is on the neurotransmitter release machinery, a concept requiring further study. Either
802 way, our electrophysiological data suggest that synaptic autophagy can function in real-time to remove
803 damaged SV proteins, contributing to the maintenance of synaptic function. This is consistent with the
804 rapid increase in presynaptic autophagy following ROS-mediated damage (Figure 3).

805 Taken together, Supernova appears to represent a powerful tool to spatiotemporally induce
806 damage to synapses and thus increase our understanding of how different clearance systems function
807 during both health and disease. This will be particularly important for the study of neurodegenerative
808 disease where the proper function of autophagy is thought to be crucial for neuronal health (Nixon,
809 2013; Rubinsztein et al., 2012).

810 References

811

812 Ashrafi, G., Schlehe, J.S., LaVoie, M.J., and Schwarz, T.L. (2014). Mitophagy of damaged mitochondria
813 occurs locally in distal neuronal axons and requires PINK1 and Parkin. *J Cell Biol* 206, 655-670.

814 Bain, J., Plater, L., Elliott, M., Shpiro, N., Hastie, C.J., McLauchlan, H., Klevernic, I., Arthur, J.S., Alessi, D.R.,
815 and Cohen, P. (2007). The selectivity of protein kinase inhibitors: a further update. *Biochem J* 408, 297-
816 315.

817 Banker, G.a.G., K. (1988). Developments in neuronal cell culture. *Nature* 336.

818 Binotti, B., Pavlos, N.J., Riedel, D., Wenzel, D., Vorbruggen, G., Schalk, A.M., Kuhnel, K., Boyken, J., Erck,
819 C., Martens, H., *et al.* (2015). The GTPase Rab26 links synaptic vesicles to the autophagy pathway. *Elife*
820 4, e05597.

821 Boland, B., Kumar, A., Lee, S., Platt, F.M., Wegiel, J., Yu, W.H., and Nixon, R.A. (2008). Autophagy
822 induction and autophagosome clearance in neurons: relationship to autophagic pathology in
823 Alzheimer's disease. *J Neurosci* 28, 6926-6937.

824 Bonanomi, D., Rusconi, L., Colombo, C.A., Benfenati, F., and Valtorta, F. (2007). Synaptophysin I
825 selectively specifies the exocytic pathway of synaptobrevin 2/VAMP2. *Biochem J* 404, 525-534.

826 Bulina, M.E., Chudakov, D.M., Britanova, O.V., Yanushevich, Y.G., Staroverov, D.B., Chepurnykh, T.V.,
827 Merzlyak, E.M., Shkrob, M.A., Lukyanov, S., and Lukyanov, K.A. (2006). A genetically encoded
828 photosensitizer. *Nat Biotechnol* 24, 95-99.

829 Carpenter, C.L., and Cantley, L.C. (1996). Phosphoinositide kinases. *Curr Opin Cell Biol* 8, 153-158.

830 Ceccarelli, B., Hurlbut, W.P., and Mauro, A. (1973). Turnover of transmitter and synaptic vesicles at the
831 frog neuromuscular junction. *J Cell Biol* 57, 499-524.

832 Chang, S., Trimbuch, T., and Rosenmund, C. (2018). Synaptotagmin-1 drives synchronous Ca(2+)-
833 triggered fusion by C2B-domain-mediated synaptic-vesicle-membrane attachment. *Nat Neurosci* 21,
834 33-40.

835 Chapman, E.R. (2002). Synaptotagmin: a Ca(2+) sensor that triggers exocytosis? *Nat Rev Mol Cell Biol*
836 3, 498-508.

837 Cheng, X.T., Zhou, B., Lin, M.Y., Cai, Q., and Sheng, Z.H. (2015a). Axonal autophagosomes recruit dynein
838 for retrograde transport through fusion with late endosomes. *J Cell Biol* 209, 377-386.

839 Cheng, X.T., Zhou, B., Lin, M.Y., Cai, Q., and Sheng, Z.H. (2015b). Axonal autophagosomes use the ride-on
840 service for retrograde transport toward the soma. *Autophagy* 11, 1434-1436.

841 Chi, P., Greengard, P., and Ryan, T.A. (2001). Synapsin dispersion and recluster during synaptic
842 activity. *Nat Neurosci* 4, 1187-1193.

843 Chu, C.T., Zhu, J., and Dagda, R. (2007). Beclin 1-independent pathway of damage-induced mitophagy
844 and autophagic stress: implications for neurodegeneration and cell death. *Autophagy* 3, 663-666.

845 Codogno, P., Mehrpour, M., and Proikas-Cezanne, T. (2011). Canonical and non-canonical autophagy:
846 variations on a common theme of self-eating? *Nat Rev Mol Cell Biol* 13, 7-12.

- 847 Cohen, L.D., Zuchman, R., Sorokina, O., Muller, A., Dieterich, D.C., Armstrong, J.D., Ziv, T., and Ziv, N.E.
848 (2013). Metabolic turnover of synaptic proteins: kinetics, interdependencies and implications for
849 synaptic maintenance. *PLoS One* 8, e63191.
- 850 Deng, Z., Purtell, K., Lachance, V., Wold, M.S., Chen, S., and Yue, Z. (2017). Autophagy Receptors and
851 Neurodegenerative Diseases. *Trends Cell Biol* 27, 491-504.
- 852 Ebrahimi-Fakhari, D., Cantuti-Castelvetri, I., Fan, Z., Rockenstein, E., Masliah, E., Hyman, B.T., McLean,
853 P.J., and Unni, V.K. (2011). Distinct roles in vivo for the ubiquitin-proteasome system and the
854 autophagy-lysosomal pathway in the degradation of alpha-synuclein. *J Neurosci* 31, 14508-14520.
- 855 Fleming, A., Noda, T., Yoshimori, T., and Rubinsztein, D.C. (2011). Chemical modulators of autophagy as
856 biological probes and potential therapeutics. *Nat Chem Biol* 7, 9-17.
- 857 Galluzzi, L., Bravo-San Pedro, J.M., Blomgren, K., and Kroemer, G. (2016). Autophagy in acute brain
858 injury. *Nat Rev Neurosci* 17, 467-484.
- 859 Gibson, D.G., Young, L., Chuang, R.-Y., Venter, J.C., Hutchison, C.A., and Smith, H.O. (2009). Enzymatic
860 assembly of DNA molecules up to several hundred kilobases. *Nature Methods* 6, 343-345.
- 861 Gordon, S.L., and Cousin, M.A. (2014). The Sybtraps: control of synaptobrevin traffic by synaptophysin,
862 alpha-synuclein and AP-180. *Traffic* 15, 245-254.
- 863 Hara, T., Nakamura, K., Matsui, M., Yamamoto, A., Nakahara, Y., Suzuki-Migishima, R., Yokoyama, M.,
864 Mishima, K., Saito, I., Okano, H., *et al.* (2006). Suppression of basal autophagy in neural cells causes
865 neurodegenerative disease in mice. *Nature* 441, 885-889.
- 866 Hernandez, D., Torres, C.A., Setlik, W., Cebrian, C., Mosharov, E.V., Tang, G., Cheng, H.C., Kholodilov, N.,
867 Yarygina, O., Burke, R.E., *et al.* (2012). Regulation of presynaptic neurotransmission by
868 macroautophagy. *Neuron* 74, 277-284.
- 869 Hilfiker, S., Pieribone, V.A., Nordstedt, C., Greengard, P., and Czernik, A.J. (1999). Regulation of
870 synaptotagmin I phosphorylation by multiple protein kinases. *J Neurochem* 73, 921-932.
- 871 Jacobson, K., Rajfur, Z., Vitriol, E., and Hahn, K. (2008). Chromophore-assisted laser inactivation in cell
872 biology. *Trends Cell Biol* 18, 443-450.
- 873 Jarvela, T.S., and Linstedt, A.D. (2014). The application of KillerRed for acute protein inactivation in
874 living cells. *Curr Protoc Cytom* 69, 12 35 11-12 35 10.
- 875 Jiang, X., Litkowski, P.E., Taylor, A.A., Lin, Y., Snider, B.J., and Moulder, K.L. (2010). A role for the
876 ubiquitin-proteasome system in activity-dependent presynaptic silencing. *J Neurosci* 30, 1798-1809.
- 877 Johansen, T.L., Trond (2011). Selective autophagy mediated by autophagic adapter proteins.
878 *Autophagy* 7, 279-296.
- 879 Kim, J.H., Lee, S.R., Li, L.H., Park, H.J., Park, J.H., Lee, K.Y., Kim, M.K., Shin, B.A., and Choi, S.Y. (2011). High
880 cleavage efficiency of a 2A peptide derived from porcine teschovirus-1 in human cell lines, zebrafish
881 and mice. *PLoS One* 6, e18556.
- 882 Klionsky, D.J., Abdalla, F.C., Abeliovich, H., Abraham, R.T., Acevedo-Arozena, A., Adeli, K., Agholme, L.,
883 Agnello, M., Agostinis, P., Aguirre-Ghiso, J.A., *et al.* (2012). Guidelines for the use and interpretation of
884 assays for monitoring autophagy. *Autophagy* 8, 445-544.
- 885 Komatsu, M., Waguri, S., Chiba, T., Murata, S., Iwata, J., Tanida, I., Ueno, T., Koike, M., Uchiyama, Y.,
886 Kominami, E., *et al.* (2006). Loss of autophagy in the central nervous system causes neurodegeneration
887 in mice. *Nature* 441, 880-884.

- 888 Lee, J.H., Yu, W.H., Kumar, A., Lee, S., Mohan, P.S., Peterhoff, C.M., Wolfe, D.M., Martinez-Vicente, M.,
889 Massey, A.C., Sovak, G., *et al.* (2010). Lysosomal proteolysis and autophagy require presenilin 1 and are
890 disrupted by Alzheimer-related PS1 mutations. *Cell* **141**, 1146-1158.
- 891 Lemasters, J.J. (2014). Variants of mitochondrial autophagy: Types 1 and 2 mitophagy and
892 micromitophagy (Type 3). *Redox Biol* **2**, 749-754.
- 893 Li, L., Tasic, B., Micheva, K.D., Ivanov, V.M., Spletter, M.L., Smith, S.J., and Luo, L. (2010). Visualizing the
894 distribution of synapses from individual neurons in the mouse brain. *PLoS One* **5**, e11503.
- 895 Liang, Y., and Sigrist, S. (2018). Autophagy and proteostasis in the control of synapse aging and
896 disease. *Curr Opin Neurobiol* **48**, 113-121.
- 897 Lilienbaum, A. (2013). Relationship between the proteasomal system and autophagy. *Int J Biochem*
898 *Mol Biol* **4**, 1-26.
- 899 Lin, J.Y., Sann, S.B., Zhou, K., Nabavi, S., Proulx, C.D., Malinow, R., Jin, Y., and Tsien, R.Y. (2013).
900 Optogenetic inhibition of synaptic release with chromophore-assisted light inactivation (CALI).
901 *Neuron* **79**, 241-253.
- 902 Linden, K.G., Liao, J.C., and Jay, D.G. (1992). Spatial specificity of chromophore assisted laser
903 inactivation of protein function. *Biophys J* **61**, 956-962.
- 904 Lois, C., Hong, E.J., Pease, S., Brown, E.J., and Baltimore, D. (2002). Germline transmission and tissue-
905 specific expression of transgenes delivered by lentiviral vectors. *Science* **295**, 868-872.
- 906 Maas, C., Torres, V.I., Altmann, W.D., Leal-Ortiz, S., Wagh, D., Terry-Lorenzo, R.T., Fejtova, A.,
907 Gundelfinger, E.D., Ziv, N.E., and Garner, C.C. (2012). Formation of Golgi-derived active zone precursor
908 vesicles. *J Neurosci* **32**, 11095-11108.
- 909 Maday, S., and Holzbaur, E.L. (2014). Autophagosome biogenesis in primary neurons follows an
910 ordered and spatially regulated pathway. *Dev Cell* **30**, 71-85.
- 911 Maday, S., Wallace, K.E., and Holzbaur, E.L. (2012). Autophagosomes initiate distally and mature
912 during transport toward the cell soma in primary neurons. *J Cell Biol* **196**, 407-417.
- 913 Martinez-Vicente, M., Tallozy, Z., Wong, E., Tang, G., Koga, H., Kaushik, S., de Vries, R., Arias, E., Harris,
914 S., Sulzer, D., *et al.* (2010). Cargo recognition failure is responsible for inefficient autophagy in
915 Huntington's disease. *Nat Neurosci* **13**, 567-576.
- 916 Mauthe, M., Orhon, I., Rocchi, C., Zhou, X., Luhr, M., Hijlkema, K.J., Coppes, R.P., Engedal, N., Mari, M., and
917 Reggiori, F. (2018). Chloroquine inhibits autophagic flux by decreasing autophagosome-lysosome
918 fusion. *Autophagy* **14**, 1435-1455.
- 919 Meberg, P.J., and Miller, M.W. (2003). Culturing hippocampal and cortical neurons. *Methods Cell Biol*
920 **71**, 111-127.
- 921 Mizushima, N., Yoshimori, T., and Levine, B. (2010). Methods in mammalian autophagy research. *Cell*
922 **140**, 313-326.
- 923 Mizushima, N., Yoshimori, T., and Ohsumi, Y. (2011). The role of Atg proteins in autophagosome
924 formation. *Annu Rev Cell Dev Biol* **27**, 107-132.
- 925 Nixon, R.A. (2013). The role of autophagy in neurodegenerative disease. *Nat Med* **19**, 983-997.

- 926 Nixon, R.A., Wegiel, J., Kumar, A., Yu, W.H., Peterhoff, C., Cataldo, A., and Cuervo, A.M. (2005). Extensive
927 involvement of autophagy in Alzheimer disease: an immuno-electron microscopy study. *J Neuropathol*
928 *Exp Neurol* **64**, 113-122.
- 929 Okerlund, N.D., Schneider, K., Leal-Ortiz, S., Montenegro-Venegas, C., Kim, S.A., Garner, L.C., Waites, C.L.,
930 Gundelfinger, E.D., Reimer, R.J., and Garner, C.C. (2017). Bassoon Controls Presynaptic Autophagy
931 through Atg5. *Neuron* **93**, 897-913 e897.
- 932 Petralia, R.S., Schwartz, C.M., Wang, Y.X., Kawamoto, E.M., Mattson, M.P., and Yao, P.J. (2013). Sonic
933 hedgehog promotes autophagy in hippocampal neurons. *Biol Open* **2**, 499-504.
- 934 Qi, Y.B.G., Emma J.; Shu, Xiaokun; Tsien, Roger Y., and Jin, Yishi (2012). Photo-inducible cell ablation in
935 *Caenorhabditis elegans* using the genetically encoded singlet
936 oxygen generating protein miniSOG. *PNAS* **109**.
- 937 Raiborg, C., and Stenmark, H. (2009). The ESCRT machinery in endosomal sorting of ubiquitylated
938 membrane proteins. *Nature* **458**, 445-452.
- 939 Rizzoli, S.O. (2014). Synaptic vesicle recycling: steps and principles. *EMBO J* **33**, 788-822.
- 940 Rubinsztein, D.C., Codogno, P., and Levine, B. (2012). Autophagy modulation as a potential therapeutic
941 target for diverse diseases. *Nat Rev Drug Discov* **11**, 709-730.
- 942 Rubinsztein, D.C., Marino, G., and Kroemer, G. (2011). Autophagy and aging. *Cell* **146**, 682-695.
- 943 Russell, R.C., Yuan, H.X., and Guan, K.L. (2014). Autophagy regulation by nutrient signaling. *Cell Res* **24**,
944 42-57.
- 945 Satoo, K., Noda, N.N., Kumeta, H., Fujioka, Y., Mizushima, N., Ohsumi, Y., and Inagaki, F. (2009). The
946 structure of Atg4B-LC3 complex reveals the mechanism of LC3 processing and delipidation during
947 autophagy. *EMBO J* **28**, 1341-1350.
- 948 Sheehan, P., Zhu, M., Beskow, A., Vollmer, C., and Waites, C.L. (2016). Activity-Dependent Degradation
949 of Synaptic Vesicle Proteins Requires Rab35 and the ESCRT Pathway. *J Neurosci* **36**, 8668-8686.
- 950 Shehata, M., Matsumura, H., Okubo-Suzuki, R., Ohkawa, N., and Inokuchi, K. (2012). Neuronal
951 stimulation induces autophagy in hippocampal neurons that is involved in AMPA receptor degradation
952 after chemical long-term depression. *J Neurosci* **32**, 10413-10422.
- 953 Shu, X., Lev-Ram, V., Deerinck, T.J., Qi, Y., Ramko, E.B., Davidson, M.W., Jin, Y., Ellisman, M.H., and Tsien,
954 R.Y. (2011). A genetically encoded tag for correlated light and electron microscopy of intact cells,
955 tissues, and organisms. *PLoS Biol* **9**, e1001041.
- 956 Soukup, S.F., Kuenen, S., Vanhauwaert, R., Manetsberger, J., Hernandez-Diaz, S., Swerts, J., Schoovaerts,
957 N., Vilain, S., Gounko, N.V., Vints, K., *et al.* (2016). A LRRK2-Dependent EndophilinA Phosphoswitch Is
958 Critical for Macroautophagy at Presynaptic Terminals. *Neuron* **92**, 829-844.
- 959 Spencer, B., Potkar, R., Trejo, M., Rockenstein, E., Patrick, C., Gindi, R., Adame, A., Wyss-Coray, T., and
960 Masliah, E. (2009). Beclin 1 gene transfer activates autophagy and ameliorates the neurodegenerative
961 pathology in alpha-synuclein models of Parkinson's and Lewy body diseases. *J Neurosci* **29**, 13578-
962 13588.
- 963 Spilman, P., Podlutskaya, N., Hart, M.J., Debnath, J., Gorostiza, O., Bredesen, D., Richardson, A., Strong, R.,
964 and Galvan, V. (2010). Inhibition of mTOR by rapamycin abolishes cognitive deficits and reduces
965 amyloid-beta levels in a mouse model of Alzheimer's disease. *PLoS One* **5**, e9979.
- 966 Stenmark, H. (2009). Rab GTPases as coordinators of vesicle traffic. *Nat Rev Mol Cell Biol* **10**, 513-525.

- 967 Takamori, S., Holt, M., Stenius, K., Lemke, E.A., Grønborg, M., Riedel, D., Urlaub, H., Schenck, S., Brügger,
968 B., Ringler, P., *et al.* (2006). Molecular anatomy of a trafficking organelle. *Cell* 127, 831-846.
- 969 Takemoto, K., Matsuda, T., Sakai, N., Fu, D., Noda, M., Uchiyama, S., Kotera, I., Arai, Y., Horiuchi, M.,
970 Fukui, K., *et al.* (2013). SuperNova, a monomeric photosensitizing fluorescent protein for
971 chromophore-assisted light inactivation. *Sci Rep* 3, 2629.
- 972 Tammineni, P., Ye, X., Feng, T., Aikal, D., and Cai, Q. (2017). Impaired retrograde transport of axonal
973 autophagosomes contributes to autophagic stress in Alzheimer's disease neurons. *Elife* 6.
- 974 Trewin, A.J., Berry, B.J., Wei, A.Y., Bahr, L.L., Foster, T.H., and Wojtovich, A.P. (2018). Light-induced
975 oxidant production by fluorescent proteins. *Free Radic Biol Med*.
- 976 Tsuruel, S., Geva, R., Zamorano, P., Dresbach, T., Boeckers, T., Gundelfinger, E.D., Garner, C.C., and Ziv,
977 N.E. (2006). Local sharing as a predominant determinant of synaptic matrix molecular dynamics. *PLoS*
978 *Biol* 4, e271.
- 979 Uytterhoeven, V., Kuenen, S., Kasprówicz, J., Miskiewicz, K., and Verstreken, P. (2011). Loss of
980 skywalker reveals synaptic endosomes as sorting stations for synaptic vesicle proteins. *Cell* 145, 117-
981 132.
- 982 Vanhauwaert, R., Kuenen, S., Masius, R., Bademosi, A., Manetsberger, J., Schoovaerts, N., Bounti, L.,
983 Gontcharenko, S., Swerts, J., Vilain, S., *et al.* (2017). The SAC1 domain in synaptotagmin is required for
984 autophagosome maturation at presynaptic terminals. *EMBO J* 36, 1392-1411.
- 985 Vijayan, V., and Verstreken, P. (2017). Autophagy in the presynaptic compartment in health and
986 disease. *J Cell Biol* 216, 1895-1906.
- 987 Vingthdeux, V., Sergeant, N., and Buee, L. (2012). Potential contribution of exosomes to the prion-like
988 propagation of lesions in Alzheimer's disease. *Front Physiol* 3, 229.
- 989 Waites, C.L., and Garner, C.C. (2011). Presynaptic function in health and disease. *Trends Neurosci* 34,
990 326-337.
- 991 Waites, C.L., Leal-Ortiz, S.A., Okerlund, N., Dalke, H., Fejtova, A., Altmann, W.D., Gundelfinger, E.D., and
992 Garner, C.C. (2013). Bassoon and Piccolo maintain synapse integrity by regulating protein
993 ubiquitination and degradation. *EMBO J* 32, 954-969.
- 994 Wang, T., Martin, S., Papadopoulos, A., Harper, C.B., Mavlyutov, T.A., Niranjana, D., Glass, N.R., Cooper-
995 White, J.J., Sibarita, J.B., Choquet, D., *et al.* (2015). Control of autophagosome axonal retrograde flux by
996 presynaptic activity unveiled using botulinum neurotoxin type a. *J Neurosci* 35, 6179-6194.
- 997 Wang, Y., Nartiss, Y., Steipe, B., McQuibban, G.A., and Kim, P.K. (2012). ROS-induced mitochondrial
998 depolarization initiates PARK2/PARKIN-dependent mitochondrial degradation by autophagy.
999 *Autophagy* 8, 1462-1476.
- 1000 Wang, Y.C., Lauwers, E., and Verstreken, P. (2017). Presynaptic protein homeostasis and neuronal
1001 function. *Curr Opin Genet Dev* 44, 38-46.
- 1002 Yang, J.Y., and Yang, W.Y. (2011). Spatiotemporally controlled initiation of Parkin-mediated mitophagy
1003 within single cells. *Autophagy* 7, 1230-1238.
- 1004 Yao, I., Takagi, H., Ageta, H., Kahyo, T., Sato, S., Hatanaka, K., Fukuda, Y., Chiba, T., Morone, N., Yuasa, S.,
1005 *et al.* (2007). SCRAPER-dependent ubiquitination of active zone protein RIM1 regulates synaptic
1006 vesicle release. *Cell* 130, 943-957.

- 1007 Ybe, J.A., Wakeham, D.E., Brodsky, F.M., and Hwang, P.K. (2000). Molecular structures of proteins
1008 involved in vesicle fusion. *Traffic* *1*, 474-479.
- 1009 Yi, J.J., and Ehlers, M.D. (2005). Ubiquitin and protein turnover in synapse function. *Neuron* *47*, 629-
1010 632.
- 1011 Yue, Z., Friedman, L., Komatsu, M., and Tanaka, K. (2009). The cellular pathways of neuronal autophagy
1012 and their implication in neurodegenerative diseases. *Biochim Biophys Acta* *1793*, 1496-1507.
- 1013 Zhu, J.H., Horbinski, C., Guo, F., Watkins, S., Uchiyama, Y., and Chu, C.T. (2007). Regulation of autophagy
1014 by extracellular signal-regulated protein kinases during 1-methyl-4-phenylpyridinium-induced cell
1015 death. *Am J Pathol* *170*, 75-86.
1016

Figure legends

Figure 1 – *Rapamycin induces rapid increase in presynaptic autophagy.*

(A) Schematic of lentiviral vector FU-Syp-mCherry-P2A-eGFP-LC3 expressing Synaptophysin (Syp)-mCherry (mCh) and eGFP-LC3 under an ubiquitin promoter. Posttranslational cleavage at the P2A site separates the two proteins.

(B) Autophagy induction (EBSS + 100 μ M chloroquine for 2 hours) of FU-Syp-mCherry-P2A-eGFP-LC3 expressing HeLa cells, demonstrating that following autophagy induction eGFP-LC3 puncta colocalize with both endogenous LC3 and p62, but not Syp-mCh.

(C) Live cell images of hippocampal neurons expressing FU-Syp-mCherry-P2A-eGFP-LC3 analyzed at 14 DIV. Syp-mCh and eGFP-LC3 exhibit different patterns indicating P2A mediated cleavage (arrow indicates Syp-mCh puncta, arrowhead indicates colocalization of Syp-mCh and eGFP-LC3).

(D) Representative images of hippocampal neurons infected with FU-Syp-mCherry-P2A-eGFP-LC3 and immunostained with antibodies against the postsynaptic protein Homer1. Colocalization of Syp-mCh and Homer1 indicate presynaptic targeting of Syp-mCh.

(E) Western Blot of lysates prepared from hippocampal neurons infected with FU-Syp-mCherry-P2A-eGFP-LC3 (TD) or uninfected (UT) and stained with mCherry antibodies. Upper band: uncleaved Syp-mCh-P2A-eGFP-LC3 fusion protein. Lower band: cleaved Syp-mCh. The lower size band representing cleaved Syp-mCh is much more abundant than the higher molecular size band representing Syp-mCh-P2A-eGFP-LC3 fusion protein, thus indicating efficient cleavage.

(F-H) Images of hippocampal neurons expressing FU-Syp-mCherry-P2A-eGFP-LC3, treated with 2 μ M rapamycin (R) for 2 hours (F) or 10 min (G and H) before fixation and staining with antibodies against p62 (H).

(I-M) Quantification of the normalized intensity of eGFP-LC3 levels at Syp-mCh puncta (I and K) as well as the number of puncta/100 μ M of axon (J and L) after 2 hours (I and J) or 10 min (K and L) of 2 μ M rapamycin treatment. (I: control = 1 ± 0.094 , n = 412 synapses, 3 independent experiments; 2 μ M R (2h) = 1.36 ± 0.164 , n = 301 synapses, 3 independent experiments, p=0.0414). (J: control = 2.72 ± 0.529 , n = 40 axons, 4 independent experiments; 2 μ M R (2h) = 4.80 ± 0.928 , n = 20 axons, 2

independent experiments, $p=0.0407$). (K: control = 1 ± 0.094 , $n = 412$ synapses, 3 independent experiments; $2\mu\text{M R (10min)} = 1.73 \pm 0.092$, $n = 343$ synapses, 3 independent experiments; $p<0.0001$). (L: control = 2.72 ± 0.529 , $n = 40$ axons, 4 independent experiments; $2\mu\text{M R (10min)} = 5.05 \pm 0.695$, $n = 47$ axons, 4 independent experiments; $p=0.0111$). Quantification of the normalized p62 levels at eGFP-LC3 puncta (M) (M: control = 1 ± 0.170 , $n = 50$ puncta, 3 independent experiments; $2\mu\text{M R (10min)} = 1.91 \pm 0.283$, $n = 52$ puncta, 3 independent experiments; $p=0.0072$) confirming that eGFP-LC3 puncta depict autophagic organelles. (N) Images of hippocampal neurons expressing FU-Syp-mCherry-P2A-eGFP-LC3 and treated with $1\mu\text{M}$ wortmannin (W) prior and during a 10 min incubation with $2\mu\text{M}$ rapamycin (R). (O and P) Quantification of (N) showing that wortmannin suppresses the induction of autophagy at Syp-mCh puncta (O) and along axons (P) following the addition of rapamycin (O: control = 1 ± 0.073 , $n = 540$ synapses, 4 independent experiments; $2\mu\text{M R (10min)} = 1.63 \pm 0.071$, $n = 469$ synapses, 4 independent experiments; $2\mu\text{M R} + 1\mu\text{M W (10min)} = 0.98 \pm 0.036$, $n = 152$ synapses, 2 independent experiments, $p<0.0001$ and $p<0.0001$). (P: control = 2.72 ± 0.529 , $n = 40$ axons, 4 independent experiments; $2\mu\text{M R (10min)} = 5.05 \pm 0.695$, $n = 47$ axons, 4 independent experiments; $2\mu\text{M R} + 1\mu\text{M W (10min)} = 1.92 \pm 0.573$, $n = 20$ axons, 2 independent experiments, $p=0.0187$ and $p=0.01$). Scale bars: $10\mu\text{m}$ (B, C and D) and $5\mu\text{m}$ (F, G, H and N). Error bars represent SEM. Unpaired T-test (I, J, K, L and M) and ANOVA Tukey's multiple comparisons test (O and P) was used to evaluate statistical significance.

Figure 2 – Rapid increase in endogenous LC3 by rapamycin treatment.

(A and B) Western Blot of lysates from cultured cortical (A) and hippocampal (B) neurons treated with $2\mu\text{M}$ rapamycin (R) for 10 min (A and B) or 2 hours (A) and stained with antibodies against Actin, Synaptophysin and LC3. Note the strong enrichment of LC3-I and LC3-II within the synaptosome suspension (syn) (left) compared to the cytosol fraction (right). Data indicate that synaptic autophagy can be rapidly induced by rapamycin treatment. (C-E) Quantification of LC3-II/Actin from the synaptosome suspensions from A (C and D) and B (E). (C: control = 0.29 ± 0.111 , 5 independent experiments; $2\mu\text{M R (10min)} = 0.44 \pm 0.101$, 5 independent

experiments). (D: control = 0.35 ± 0.178 , 3 independent experiments; $2\mu\text{M R (2h)} = 0.84 \pm 0.200$, 3 independent experiments). (E: control = 0.13 ± 0.029 , 3 independent experiments; $2\mu\text{M R (10min)} = 0.50 \pm 0.173$, 3 independent experiments).

Error bars represent SEM. Unpaired T-test was used to evaluate statistical significance.

Figure 3 – Rapid induction of autophagy by ROS-mediated damage by Synaptophysin-Supernova.

(A) Schematic of FU-Syp-Supernova-P2A-eGFP-LC3 expression vector.

(B) Low-magnification images of hippocampal neurons expressing FU-Syp-Supernova-P2A-eGFP-LC3 grown on top of uninfected neurons before and after photobleaching a region of interest (dashed line). Boxes represent areas within (red) and outside (black) bleached area used for analysis.

(C-E) Images of axon segments (5 min, 1 hour and 2 hours after bleaching) that were subsequently fixed and stained with antibodies against GFP to detect eGFP-LC3 and Supernova to detect Syp-SN. Data indicate that autophagy at synapses can be rapidly induced through Syp-SN photobleaching.

(F) Quantification of normalized eGFP-LC3 intensities within Syp-SN puncta 5 min (C) after bleaching (unbleached = 1 ± 0.057 , n = 119 synapses, 3 independent experiments; bleached = 1.43 ± 0.113 , n = 132 synapses, 3 independent experiments, $p=0.001$).

(G) Quantification of the normalized number of eGFP-LC3 puncta per unit axon length, in axons 5 min after photobleaching (C) (unbleached = 1 ± 0.166 , n = 17 axons, 3 independent experiments; bleached = 0.70 ± 0.119 , n = 18 axons, 3 independent experiments).

(H) Quantification of normalized eGFP-LC3 intensities within Syp-SN puncta 1 hour (D) after bleaching (unbleached = 1 ± 0.071 , n = 132 synapses, 3 independent experiments; bleached = 1.43 ± 0.117 , n = 167 synapses, 3 independent experiments, $p=0.0035$).

(I) Quantification of the normalized number of eGFP-LC3 puncta per unit axon length in axons 1 hour after photobleaching (D) (unbleached = 1 ± 0.146 , n = 24 axons, 3 independent experiments; bleached = 1.37 ± 0.166 , n = 24 axons, 3 independent experiments).

(J) Quantification of normalized eGFP-LC3 intensities within Syp-SN puncta 2 hours (E) after bleaching (unbleached = 1 ± 0.054 , n = 136 synapses, 3 independent experiments; bleached = 1.22 ± 0.065 , n = 141 synapses, 3 independent experiments, $p=0.0111$).

(K) Quantification of the normalized number of eGFP-LC3 puncta per unit axon length 2 hours after photobleaching (E) (unbleached = 1 ± 0.173 , $n = 23$ axons, 3 independent experiments; bleached = 2.75 ± 0.336 , $n = 22$ axons, 3 independent experiments, $p < 0.0001$).

Scale bars: $50\mu\text{m}$ (B), $10\mu\text{m}$ (C, D and E). Error bars represent SEM. Unpaired T-test was used to evaluate statistical significance.

Figure 4 – Bleaching-induced increase in eGFP-LC3 levels at presynaptic boutons is ROS-dependent.

(A) Images of untransfected (UT) HEK293 cells or those expressing FU-Syp-mCherry-P2A-eGFP-LC3 (mCherry/mCh) or FU-Syp-Supernova-P2A-eGFP-LC3 (Supernova/SN) before and 15 minutes after 60 seconds photobleaching. Cells were treated with $10\mu\text{M}$ dihydroethidium 20 minutes before bleaching.

(B) Quantification of the decrease in DHE_{blue} intensity upon bleaching (UT = 51.08 ± 5.566 , $n = 26$ cells, 3 independent experiments; mCh = 102 ± 12.680 , $n = 36$ cells, 4 independent experiments; SN = 157 ± 21.310 , $n = 31$ cells, 4 independent experiments, $p < 0.0001$ and $p = 0.0253$).

(C, D and E) Images of hippocampal neurons expressing FU-Syp-mCherry-P2A-eGFP-LC3 (C), FU-Syp-Supernova-P2A-eGFP-LC3 (D and E) that were fixed and stained with antibodies against GFP and Supernova/mCherry (XY) 1 hour after photobleaching, either in the absence (C and D) or presence of $60\mu\text{M}$ N-acetyl-L-cysteine (NAC) (E).

(F) Quantification of normalized eGFP-LC3 intensities within Syp-XY puncta (mCh = 1.15 ± 0.049 , $n = 489$ synapses, 4 independent experiments; SN = 1.37 ± 0.056 , $n = 450$ synapses, 4 independent experiments; SN + NAC = 1.18 ± 0.057 , $n = 198$ synapses, 3 independent experiments, $p = 0.0049$).

Scale bars: $20\mu\text{m}$ (A) and $10\mu\text{m}$ (C, D and E). Error bars represent SEM. ANOVA Tukey's multiple comparisons test was used to evaluate statistical significance.

Figure 5 – Rapid increase in endogenous LC3 by bleaching of Syp-Supernova.

(A) Schematic of FU-Syp-Supernova expression vector.

(B-D) Images of hippocampal neurons expressing FU-Syp-Supernova that were fixed and stained with antibodies against LC3 and Bassoon 5 min, 1 hour and 2 hours after bleaching. Data indicate that autophagy at synapses can be rapidly induced through Syp-SN photobleaching.

(E) Quantification of normalized LC3 intensities within Syp-SN/Bsn puncta 5 min (B) after bleaching (unbleached = 1 ± 0.077 , $n = 74$ synapses, 3 independent experiments; bleached = 1.50 ± 0.126 , $n = 75$ synapses, 3 independent experiments, $p=0.0011$).

(F) Quantification of normalized LC3 intensities within Syp-SN/Bsn puncta 1 hour (C) after bleaching (unbleached = 1 ± 0.072 , $n = 59$ synapses, 3 independent experiments; bleached = 1.31 ± 0.092 , $n = 49$ synapses, 3 independent experiments, $p=0.0093$).

(G) Quantification of normalized LC3 intensities within Syp-SN/Bsn puncta 2 hours (D) after bleaching (unbleached = 1 ± 0.069 , $n = 60$ synapses, 3 independent experiments; bleached = 1.43 ± 0.101 , $n = 60$ synapses, 3 independent experiments, $p=0.0006$).

Scale bars: $10\mu\text{m}$. Error bars represent SEM. Unpaired T-test was used to evaluate statistical significance.

Figure 6 – ROS-induced increase in eGFP-LC3 levels at presynaptic boutons is PI3K- and Atg5-dependent.

(A and B) Images of hippocampal neurons expressing FU-Syp-Supernova-P2A-eGFP-LC3 that were fixed and stained with antibodies against GFP and Supernova 2 hours after photobleaching, either in the absence (A) or presence of $1\mu\text{M}$ wortmannin (W) (B).

(C and D) Quantification of normalized eGFP-LC3 intensities within Syp-SN puncta (C) or the normalized number of eGFP-LC3 puncta per unit axon length (D) in bleached and unbleached areas (C: unbleached = 1 ± 0.057 , $n = 174$ synapses, 3 independent experiments; bleached = 1.22 ± 0.073 , $n = 174$ synapses, 3 independent experiments, $p=0.0173$) (D: unbleached = 1 ± 0.221 , $n = 19$ axons, 3 independent experiments; bleached = 2.35 ± 0.403 , $n = 21$ axons, 3 independent experiments, $p=0.0071$).

(E and F) Quantification of normalized eGFP-LC3 intensities within Syp-SN puncta (E) or number of eGFP-LC3 puncta per unit axon length (F) in culture treated with wortmannin before and after photobleaching. (E: unbleached = 1 ± 0.057 , $n = 179$ synapses, 3 independent experiments; bleached = 0.95 ± 0.055 , $n = 164$ synapses, 3 independent experiments). (F: unbleached = 1 ± 0.228 , $n = 18$ axons, 3 independent experiments; bleached = 2.22 ± 0.348 , $n = 21$ axons, 3 independent experiments, $p=0.0077$).

(G and H) Images of hippocampal neurons expressing F-U6-scRNA(SC)-U-Syp-Supernova-P2A-eGFP-LC3 (G) or F-U6-shAtg5-U-Syp-Supernova-P2A-eGFP-LC3 (H) that were fixed and stained with antibodies against GFP and Supernova 2 hours after photobleaching.

(I and J) Quantification of normalized eGFP-LC3 intensities within Syp-SN puncta (I) or the normalized number of eGFP-LC3 puncta per unit axon length (J) in cultures expressing F-U6-scRNA(SC)-U-Syp-Supernova-P2A-eGFP-LC3. (I: unbleached = 1 ± 0.058 , $n = 134$ synapses, 3 independent experiments; bleached = 1.35 ± 0.073 , $n = 178$ synapses, 3 independent experiments, $p=0.0001$) (J: unbleached = 1 ± 0.090 , $n = 27$ axons, 3 independent experiments; bleached = 1.67 ± 0.107 , $n = 27$ axons, 3 independent experiments, $p<0.0001$).

(K and L) Quantification of normalized eGFP-LC3 intensities within Syp-SN puncta (K) or number of eGFP-LC3 puncta per unit axon length (L) in cultures expressing F-U6-shAtg5-U-Syp-Supernova-P2A-eGFP-LC3. (K: unbleached = 1 ± 0.052 , $n = 109$ synapses, 3 independent experiments; bleached = 0.98 ± 0.055 , $n = 127$ synapses, 3 independent experiments). (L: unbleached = 1 ± 0.103 , $n = 27$ axons, 3 independent experiments; bleached = 1.22 ± 0.122 , $n = 27$ axons, 3 independent experiments).

Scale bars: 10 μ m. Error bars represent SEM. Unpaired T-test was used to evaluate statistical significance.

Figure 7 – *Syp-Supernova mediated ROS production increases autophagic vacuoles (AVs) in presynaptic terminals.*

(A and B) Example EM micrographs of organelles quantified as autophagic vacuoles (AVs) (A) or multivesicular bodies (MVBs) (B).

(C and F) Representative EM micrographs of unbleached or bleached synapses 10 (C) or 40 (F) min after photobleaching. Arrowheads indicate double-membraned AVs. Note, # of AVs but not MVBs is significantly increased 10 min following Syp-SN mediated ROS production.

(D and E) Quantification of the number of AVs (D) or MVBs (E) per terminal 10 min after photobleaching (D: unbleached = 0.05 ± 0.018 , $n = 228$ synapses, 1 independent experiments; bleached = 0.17 ± 0.044 , $n = 198$ synapses, 2 independent experiments, $p=0.0062$) (E: unbleached =

1183 0.04 ± 0.013 , $n = 228$ synapses, 2 independent experiments; bleached = 0.05 ± 0.016 , $n = 198$ synapses,
1184 2 independent experiments).

1185 (G and H) Quantification of the number of AVs (G) or MVBs (H) per terminal 40 min after
1186 photobleaching (G: unbleached = 0.04 ± 0.016 , $n = 138$ synapses, 2 independent experiments;
1187 bleached = 0.09 ± 0.028 , $n = 215$ synapses, 2 independent experiments) (H: unbleached = 0.05 ± 0.019 ,
1188 $n = 138$ synapses, 2 independent experiments; bleached = 0.05 ± 0.014 , $n = 215$ synapses, 2
1189 independent experiments).

1190 Scale bars: 300nm (C and F), 200nm (A and B). Error bars represent SEM. Unpaired T-test was used to
1191 evaluate statistical significance.

1192

1193 **Figure 8** – *Syp-Supernova mediated ROS production increases eGFP-Rab7 and Chmp2b levels at*
1194 *presynaptic boutons.*

1195 (A) Schematic of FU-Syp-Supernova-P2A-eGFP-Rab7 expression vector.

1196 (B, C and D) Images of hippocampal neurons expressing FU-Syp-Supernova-P2A-eGFP-Rab7 that were
1197 fixed and stained with antibodies against GFP, Supernova and Chmp2b, 5 min, 1 hour and 2 hours after
1198 Syp-SN mediated ROS production.

1199 (E, G and I) Quantification of the normalized eGFP-Rab7 intensity in Syp-SN puncta 5 min, 1 hour or 2
1200 hours after photobleaching of Syp-SN (E: unbleached = 1 ± 0.052 , $n = 249$ synapses, 4 independent
1201 experiments; bleached = 1.24 ± 0.066 , $n = 314$ synapses, 4 independent experiments, $p=0.0063$) (G:
1202 unbleached = 1 ± 0.050 , $n = 280$ synapses, 4 independent experiments; bleached = 1.16 ± 0.053 , $n =$
1203 373 synapses, 4 independent experiments, $p=0.0376$) (I: unbleached = 1 ± 0.046 , $n = 258$ synapses, 4
1204 independent experiments; bleached = 1.40 ± 0.083 , $n = 352$ synapses, 4 independent experiments,
1205 $p=0.0001$). Note, Rab7 levels are significantly increased at all three times.

1206 (F, H and J) Quantification of the normalized Chmp2b intensity in Syp-SN puncta 5 min, 1 hour or 2
1207 hours after photobleaching of Syp-SN. Levels are significantly increased at 1 hour but not 5 min or 2
1208 hours after ROS-mediated damage. (F: unbleached = 1 ± 0.089 , $n = 67$ synapses, 2 independent
1209 experiments; bleached = 1.44 ± 0.219 , $n = 71$ synapses, 2 independent experiments) (H: unbleached =
1210 1 ± 0.080 , $n = 91$ synapses, 2 independent experiments; bleached = 1.45 ± 0.174 , $n = 89$ synapses, 2

independent experiments, $p=0.0196$) (J: unbleached = 1 ± 0.074 , $n = 108$ synapses, 2 independent experiments; bleached = 1.23 ± 0.134 , $n = 118$ synapses, 2 independent experiments).

Scale bars: $10\mu\text{m}$. Error bars represent SEM. Unpaired T-test was used to evaluate statistical significance.

Figure 9 – *Syt-Supernova and Syn-Supernova mediated ROS production increases eGFP-LC3 levels at presynaptic boutons.*

(A) Schematic of a SV containing Synaptophysin (Syp), Synaptotagmin (Syt) or Synapsin (Syn) tagged with Supernova. Note, the short (95aa) (Gordon and Cousin, 2014) vs. long (346aa, comprised of two C2 domains) (Ybe et al., 2000) cytoplasmic tails of Synaptophysin vs. Synaptotagmin, respectively, which could significantly change the distance of Supernova to the SV membrane and thus its proximity to other SV proteins. Similarly, tagging Supernova to the much larger peripherally associated SV protein Synapsin could also affect its distance to other SV proteins.

(B, C and D) Images of hippocampal neurons expressing FU-Syt-Supernova-P2A-eGFP-LC3 that were fixed and stained with antibodies against GFP and Supernova 5 min (B), 1 hour (C) and 2 hours (D) after bleaching. Note, eGFP-LC3 levels are significantly increased 1 hour after Synaptotagmin-Supernova (Syt-SN) mediated ROS production.

(E, F and G) Quantification of normalized eGFP-LC3 intensities within Syt-SN puncta, 5 min (E), 1 hour (F) and 2 hours (G) after bleaching. (E: unbleached = 1 ± 0.074 , $n = 62$ synapses, 2 independent experiments; bleached = 1.06 ± 0.098 , $n = 76$ synapses, 2 independent experiments) (F: unbleached = 1 ± 0.111 , $n = 73$ synapses, 2 independent experiments; bleached = 1.45 ± 0.143 , $n = 81$ synapses, 2 independent experiments, $p=0.0156$) (G: unbleached = 1 ± 0.085 , $n = 58$ synapses, 2 independent experiments; bleached = 1.05 ± 0.087 , $n = 68$ synapses, 2 independent experiments).

(H, I and J) Images of hippocampal neurons expressing FU-Syn-Supernova-P2A-eGFP-LC3 that were fixed and stained with antibodies against GFP and Supernova 5 min (H), 1 hour (I) and 2 hours (J) after bleaching. Note, eGFP-LC3 levels are significantly increased 1 hour and 2 hours after Synapsin-Supernova (Syn-SN) mediated ROS production.

(K, L and M) Quantification of normalized eGFP-LC3 intensities within Syn-SN puncta, 5 min (K), 1 hour (L) and 2 hours (M) after bleaching. (K: unbleached = 1 ± 0.084 , n = 58 synapses, 3 independent experiments; bleached = 1.04 ± 0.069 , n = 81 synapses, 3 independent experiments) (L: unbleached = 1 ± 0.061 , n = 77 synapses, 3 independent experiments; bleached = 1.72 ± 0.103 , n = 103 synapses, 3 independent experiments, $p < 0.0001$) (M: unbleached = 1 ± 0.075 , n = 42 synapses, 3 independent experiments; bleached = 1.30 ± 0.090 , n = 71 synapses, 3 independent experiments, $p = 0.0255$). Scale bars: 10 μ m. Error bars represent SEM. Unpaired T-test was used to evaluate statistical significance.

Figure 10 – ROS-damaged SV proteins selectively accumulate in autophagy organelles.

(A, B and C) Images of hippocampal neurons expressing Supernova-tagged synaptic proteins Syp-SN (A), Syp-SN (B) or Syp-lumSN (C) that were fixed 1 hour after bleaching and stained with antibodies against GFP, Supernova, Bassoon and Synaptotagmin1 (Syt1) (A and C) or Synaptophysin1 (Syp1) (B).

(D) Quantification of the fraction of extrasynaptic eGFP-LC3 puncta positive for SN-tagged Synaptophysin, indicated by arrowheads in (A), or endogenous Syt1 within the same experiment (Syp-SN = 0.71 ± 0.075 , n = 38 puncta, 3 independent experiments; Syt1 = 0.18 ± 0.064 , n = 38 puncta, 3 independent experiments, $p < 0.0001$). Also quantified is the fraction of extrasynaptic Syp-SN puncta that are positive for eGFP-LC3 (0.43 ± 0.060 , n = 68 puncta, 3 independent experiments).

(E) Quantification of the fraction of extrasynaptic eGFP-LC3 puncta positive for SN-tagged Synaptotagmin, indicated by arrowheads (B), or endogenous Syp1 within the same experiment (Syp-SN = 0.70 ± 0.081 , n = 33 puncta, 2 independent experiments; Syp1 = 0.18 ± 0.068 , n = 33 puncta, 2 independent experiments, $p < 0.0001$). Also quantified is the fraction of extrasynaptic Syp-SN puncta that are positive for eGFP-LC3 (0.43 ± 0.068 , n = 54 puncta, 2 independent experiments).

(F) Quantification of the fraction of extrasynaptic eGFP-LC3 puncta positive for luminal SN-tagged Synaptophysin (Syp-lumSN), indicated by arrowheads in (C), or endogenous Syt1 within the same experiment (Syp-lumSN = 0.08 ± 0.033 , n = 66 puncta, 3 independent experiments; Syt1 = 0.17 ± 0.046 , n = 66 puncta, 3 independent experiments). Also quantified is the fraction of extrasynaptic Syp-

lumSN puncta that are positive for eGFP-LC3 (0.51 ± 0.077 , $n = 43$ puncta, 3 independent experiments).

(G) Images of hippocampal neurons expressing FU-eGFP-LC3 fixed and stained with antibodies against GFP, Bassoon and Synaptophysin1 (Syp1), or Synapsin1 (Syn1), or Synaptotagmin1 (Syt1).

(H) Quantification of the fraction of extrasynaptic eGFP-LC3 puncta also positive for endogenous Synaptophysin1, Synapsin1 or Synaptotagmin1. Note, the fraction of extrasynaptic eGFP-LC3 puncta positive for Synaptophysin1 is significantly higher than the fraction positive for Synapsin1 (Syp1 basal = 0.40 ± 0.051 , $n = 93$ puncta, 2 independent experiments; Syn1 basal = 0.14 ± 0.038 , $n = 85$ puncta, 2 independent experiments; Syt1 basal = 0.28 ± 0.050 , $n = 81$ puncta, 2 independent experiments).

Scale bars: $10\mu\text{m}$. Error bars represent SEM. Unpaired T-test (D, E and F) and ANOVA Tukey's multiple comparisons test (H) was used to evaluate statistical significance.

1276

Figure 11 – *ROS-induced damage to Syp-SN impairs evoked release only when autophagy is inhibited.*

(A, B and C) Example traces of whole-cell patch recording of evoked EPSCs from autaptic hippocampal neurons expressing FU-Syp-Supernova-P2A-eGFP-LC3 before and 5 min after ROS-induced damage to Syp-SN either in the absence (A) or presence of $1\mu\text{M}$ wortmannin (W) (C). Neurons treated with wortmannin but were not bleached served as a control (B). (A. amplitude: before = 4.25 ± 1.050 , after = 3.74 ± 1.134 , 14 neurons, 3 independent experiments) (B. amplitude: before = 2.07 ± 0.311 , after = 1.85 ± 0.277 , 13 neurons, 3 independent experiments) (C. amplitude: before = 2.50 ± 0.570 , after = 1.63 ± 0.409 , 16 neurons, 3 independent experiments, $p=0.0042$).

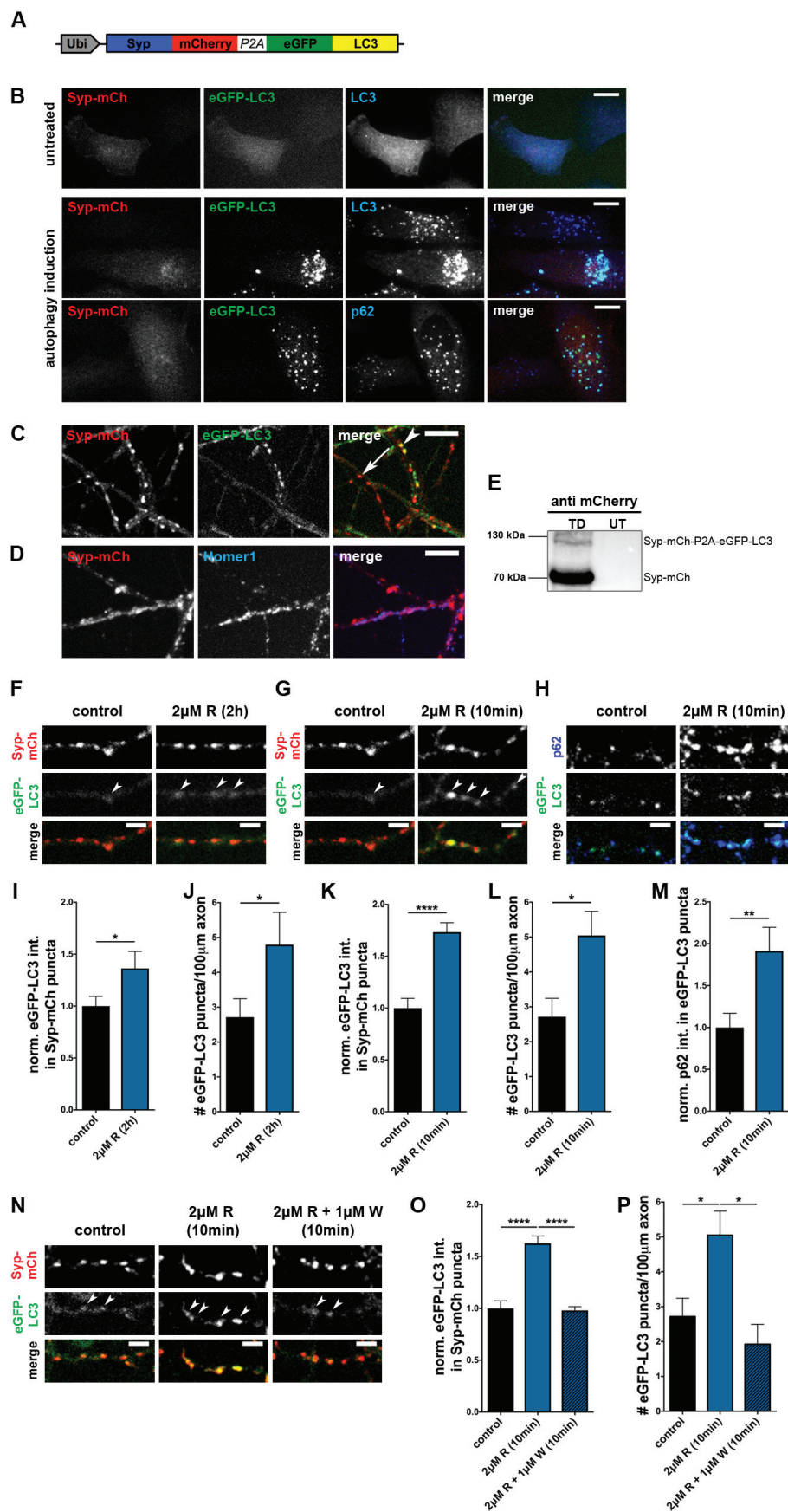
(D) Quantification of the percent decrease in EPSC amplitude after photobleaching (A and C) or waiting period (B). Note that the decrease in amplitude is significantly higher when $1\mu\text{M}$ wortmannin is present (bleached = 14.57 ± 6.620 , $n = 14$ neurons, 3 independent experiments; $1\mu\text{M}$ W = 11.09 ± 8.479 , $n = 13$ neurons, 3 independent experiments; $1\mu\text{M}$ W bleached = 39.69 ± 6.869 , $n = 16$ neurons, 3 independent experiments, $p=0.0445$ and $p=0.0223$).

(E, F and G) Example traces of whole-cell patch recording of evoked EPSCs from autaptic hippocampal neurons expressing F-U6-scRNA(SC)-U-Syp-Supernova-P2A-eGFP-LC3 (E) or F-U6-shAtg5-U-Syp-Supernova-P2A-eGFP-LC3 (G) before and 5 min after ROS-induced damage to Syp-SN. Neurons

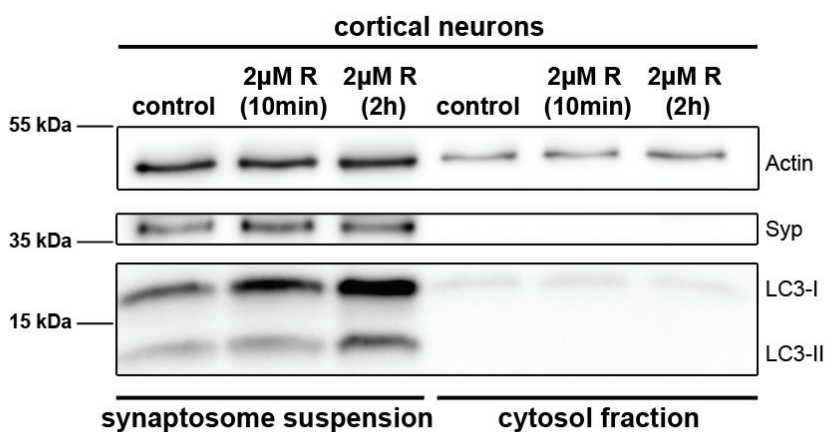
1293 expressing F-U6-shAtg5-U-Syp-Supernova-P2A-eGFP-LC3 that were not bleached served as a control
1294 (F). (E amplitude: before = 4.23 ± 0.853 , after = 3.87 ± 0.980 , 17 neurons, 3 independent experiments)
1295 (F amplitude: before = 4.60 ± 0.987 , after = 4.22 ± 0.962 , 16 neurons, 3 independent experiments) (G
1296 amplitude: before = 5.58 ± 0.800 , after = 3.79 ± 0.687 , 16 neurons, 3 independent experiments,
1297 $p < 0.0001$).

1298 (H) Quantification of the percent decrease in EPSC amplitude after photobleaching (E and G) or
1299 waiting period (F). Note that the decrease in amplitude is significantly higher in F-U6-shAtg5-U-Syp-
1300 Supernova-P2A-eGFP-LC3 expressing neurons that were bleached (SC bleached = 11.15 ± 7.261 , $n = 17$
1301 neurons, 3 independent experiments; shAtg5 = 5.74 ± 5.836 , $n = 16$ neurons, 3 independent
1302 experiments; shAtg5 bleached = 38.19 ± 5.766 , $n = 16$ neurons, 3 independent experiments, $p = 0.0114$
1303 and $p = 0.0024$).

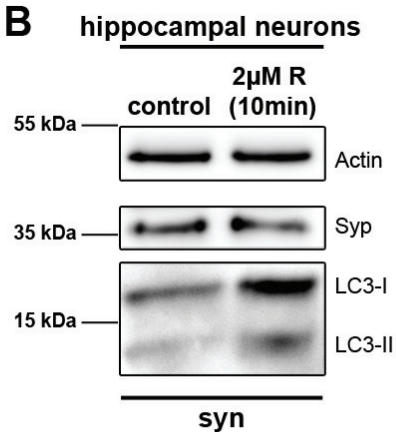
1304 Error bars represent SEM. Paired T-test (A-C, E-G) and ANOVA Tukey's multiple comparisons test (D
1305 and H) was used to evaluate statistical significance.



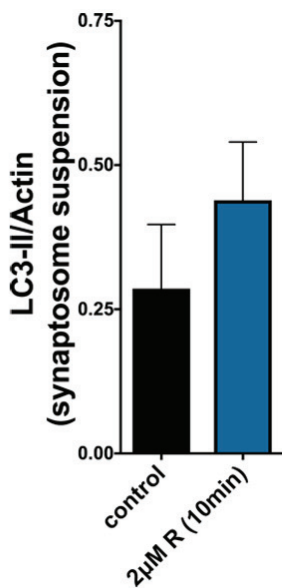
A



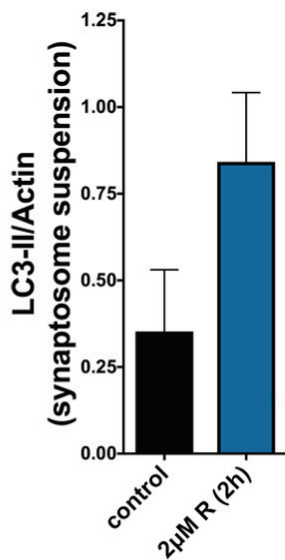
B



C



D



E

